BACHELOR

Efimov physics for a finite square well potential

Mestrom, P.M.A.

Award date:
2015

Efimov physics for a finite square well potential

P.M.A. Mestrom
Student number: 0796893

June 30, 2015

Bachelor Thesis

Supervisor: dr. ir. S.J.J.M.F. Kokkelmans

Applied Physics:
Coherence and Quantum Technology

Eindhoven University of Technology

Abstract

The most important goal of this bachelor thesis is to calculate the Efimov spectrum for a square well potential as two-body interaction and to investigate the universality of the three-body parameter $a_0^{(-)}$. Since inelastic collisions should be incorporated into Efimov physics, the off-shell two-body T-matrix of the square well potential is calculated first. The obtained T-matrix is used as input for the Skorniakov-Ter-Martirosian equation from which the Efimov bound states can be calculated.

The off-shell two-body T-matrix for s-wave scattering depends on the momentum of the incoming wave, the momentum of the scattered wave and on the energy of the two-particle system. It is symmetric under the exchange of the ingoing and outgoing momenta.

An import characteristic of the off-shell T-matrix is that at higher order resonances, i.e. $K_0R = n\pi/2$ with n = 3, 5, 7, etc., the absolute maximum of the T-matrix does not occur at $k'R = 0$ even if the absolute values of kR and qR are close to zero. In this case the maximum peak occurs at $k'R = K_0R$.

The Efimov spectrum for a zero-range interaction potential is characterized by a universal scaling behavior of the trimer states. However, finite range effects of the interaction potential can lead to both non-universality in the scaling factor, especially for the lowest energy Efimov states, and a three-body parameter which cuts off the Efimov spectrum from below.

The Efimov spectrum is calculated for the resonance condition $K_0R = \pi/2$. It is shown that the deviation of the first scaling factor ($a_1^{(-)}/a_0^{(-)} = 18$) from the universal scaling factor 22.7 is probably the result of finite range effects. A surprising result of the Efimov spectrum is the absence of the parameter $a_0^{(+)}$ which means that the energy of the lowest-energy three-body bound state does not converge to the two-body bound state energy.

The three-body parameter of the lowest-energy trimer state has also been found for the resonance condition $K_0R = \pi/2$. It value is $a_0^{(-)} = -3R$, so it does not equal the universal three-body parameter $a_0^{(-)} = -9.8\,R_{vdW}$ which is experimentally observed. The universal value of $a_0^{(-)}$ is more likely to be retrieved for deeper square well potentials. Further research is needed to confirm this hypothesis.

Table of Contents

1. Introduction 1

2. The Efimov effect 3

3. Resonances in two-body collisions 6
   3.1 Potential resonance 6
   3.2 Coupling of different spin channels 6
   3.3 Feshbach resonance 7

4. Two-body scattering theory 8
   4.1 Two-particle systems 8
   4.2 Lippmann-Schwinger equation 8
   4.3 Scattering operator 9
   4.4 Transition operator 10
   4.5 S-matrix and T-matrix 10
   4.6 Off-shell wave function 11
   4.7 Spherical-wave states 12
   4.8 Partial wave analysis for on-shell scattering 13
   4.9 Ultracold limit 13
   4.10 Normalization 14

5. Three-body scattering theory 15
   5.1 Jacobi coordinates 15
   5.2 Skorniakov-Ter-Martirosian equation 15

6. S-wave scattering by a finite square well potential 17
   6.1 S-wave scattering ($E > 0$) 17
   6.2 Low energy bound states ($E < 0$) 19
   6.3 S-matrix and on-shell T-matrix of the square well potential 19
   6.4 Half-off-shell T-matrix of the square well potential 20
   6.5 Off-shell wave function of the square well potential 22
   6.6 Off-shell T-matrix of the square well potential 23

7. Model setup 26
7.1 The angular dependence of the STM-equation 26
7.2 STM-equation for a square well potential 26
7.3 Efimov trimer states 27
7.4 Dissociation threshold 28

8. Results and discussion 29

9. Conclusion 35

Appendix A: Justification for neglecting partial waves with nonzero angular momenta 37

Appendix B: Additional figures of the off-shell T-matrix 39

Appendix C: Comparison with Rademaker's model 40

Appendix D: Angular dependence of the STM-equation 42
D.1 Justification of Levinsen's approximation 42
D.2 Derivation of Eq. (7.1) 43

References 44

1. Introduction

In the early seventies Vitaly Efimov studied the situation of three identical bosons with resonant attractive two-body interactions. These three particles exhibit an infinite sequence of three-body bound states when the two-body scattering length diverges (Efimov, 1970), (Braaten & Hammer, 2006). These trimers can also exist in the regime in which no two-body bound states exist. This remarkable result is comparable with the Borromean rings. These three rings form a bound state although the two-body sub-systems are unbound. The first experimental evidence for Efimov states was given by a research group at the University of Innsbruck in 2006 (Kraemer et al., 2006) who used an ultracold gas of cesium atoms.

Finite range potentials always have a deepest lying Efimov state which can be characterized by a three-body parameter $a_0^{(-)}$. Efimov predicted a universal scaling behavior of the trimer states. However, finite range effects of the interaction potential can lead to non-universality in the scaling factor, especially for the deepest lying Efimov states. Furthermore, there will be a three-body parameter that cuts off the Efimov spectrum from below. Recent experiments with different atomic species have shown that the three-body parameter is universal when measured in units of an effective range and that the finite-range nature of the interaction plays a crucial rule in the universality of the three-body parameter (Horinouchi & Ueda, 2015).

The goal of the bachelor thesis is to calculate the Efimov spectrum for a square well potential as two-body interaction and to investigate the universality of the three-body parameter. This simple interaction potential will be used because many features of the square well potential are common to more complicated finite range potentials. One of these features is the divergence of the scattering length for specific values of the depth and width of the square well. This potential resonance, which is a purely s-wave phenomenon, has therefore similarities with the Feshbach resonance which is used to precisely tune the two-body interactions via an external magnetic field. In this way the Efimov bound states can be experimentally observed. It is important to incorporate inelastic collisions into Efimov physics. Therefore three-body collisions require knowledge of the fully off-shell two-body T-matrix over the entire momentum space. Since at low energies scattering with a finite range potential is dominated by s-wave scattering (Sakurai, 1994), only the s-wave contribution to the fully off-shell two-body T-matrix is needed.

The report can be subdivided into two parts. The first part is analytical. The goal of this part is to obtain the off-shell two-body T-matrix for s-wave scattering by a square well potential. In order to calculate this T-matrix the off-shell wave function should be determined. This wave function is calculated from the off-shell analog of the Lippmann-Schwinger equation. This analytical part of my bachelor thesis encompasses 10 ECTS.

In the second part, which is the extension of my bachelor thesis, the three-body scattering problem for three identical low energy bosons is considered. The obtained off-shell two-body T-matrix is used as input for the Skorniakov-Ter-Martirosian (STM) equation from which the Efimov bound states can be calculated. The STM-equation is a Fredholm integral equation of the second kind. Therefore it has to be solved numerically. This numerical part of my bachelor thesis encompasses 5 ECTS.

The research question of my extension is as follows:
How does the Efimov spectrum look like taking into account the fully off-shell two-body T-matrix of the square well potential and what is the corresponding three-body parameter?

The report starts with more background theory about the Efimov effect. Next, two resonance phenomena, the Feshbach resonance and the potential resonance, will be described. The theory of two-body scattering processes is given in chapter 4. This chapter describes how the two-body off-shell T-matrix can be calculated. The simplified STM-equation for low energy atom-dimer scattering is given in chapter 5. S-wave scattering by a finite square well potential is analyzed in chapter 6. Here the off-

shell T-matrix of the square well potential will be calculated. The potential resonance of the square well potential is used to simulate a Feshbach resonance. The model setup is given in chapter 7. In the next chapter, the model is used to calculate the Efimov spectrum and to investigate the universality of the three-body parameter. Chapter 5, 7 and 8 are part of the extension of my bachelor thesis. Finally, the conclusion summarizes the most important results and a list of literature references is given.

2. The Efimov effect

The Efimov effect is a fundamental property of quantum three-body systems predicted by the Russian theoretical physicist Vitaly Efimov in the early seventies. He predicted that a system of three identical bosons with resonant two-body interactions features an infinite series of three-body bound states (Efimov, 1970), (Braaten & Hammer, 2006). These Efimov trimer states are universal in the sense that they are independent of the short-range details of the two-body interactions. Due to this universality experimentalists have tried to observe the Efimov effect in many different systems such as three-body bound states of Helium-4, triton compounds and ultracold quantum gases (Ferlaino et al., 2011). Up to 2006 Efimov states could not be observed experimentally. However, a research group at the University of Innsbruck (Kraemer et al., 2006) gave the first experimental evidence for Efimov states in an ultracold gas of cesium atoms in 2006. Since then, many experiments with ultracold gases have given clear evidence of the existence of the Efimov effect (Ferlaino et al., 2011).

Efimov thought that the Efimov states could exist in systems of three α-particles (^{12}C nucleus) and three nucleons (^{3}H nucleus) (Efimov, 1970). However, the Efimov effect has not been observed yet in in these systems because the experiments are difficult to conduct.

Due to their unique properties ultracold quantum gasses are very useful for experimentally studying the physics of Efimov states. Ultracold quantum gasses provide an unprecedented level of control. Since the collision energies are extremely low, the details of the short-range interaction become irrelevant because of the long-range nature of the wave function (Sakurai, 1994). Therefore s-wave scattering dominates the two-body interactions. As a result, the two-body physics is completely characterized by the s-wave scattering length (Sakurai, 1994). Therefore the two-body interactions can be precisely tuned via an external magnetic field on the basis of Feshbach resonances which will be described in chapter 3 (Feshbach, 1958).

Fig. 2.1 shows the energy spectrum of the three-body system as a function of the inverse scattering length $1/a$. For $a < 0$ trimer states can exist for energies below zero. However, for $E > 0$ the states are continuum states of three free atoms. The region in which $a < 0$ is called the Borromean region (Ferlaino et al., 2011). This name refers to the Borromean rings. Three rings can form a bound state although the two-body sub-systems are unbound. Similarly dimer states do not exist in the Borromean region. However, for $a > 0$ dimer states can also exist and the dissociation threshold for three atoms at rest is given by

$$E = -\frac{\hbar^2}{ma^2}. \tag{2.1}$$

Here m is the mass of the atom and $\hbar$ is the reduced Planck constant. The threshold energy given by eq. (2.1) is the universal binding energy of a weakly bound dimer and it is indicated in Fig. 2.1 by the blue curve. All states below this threshold are the discrete three-body bound states which dissociate into a dimer and an atom when the energy equals the threshold energy given by Eq. (2.1). According to Efimov there would be an infinite sequence of weakly bound trimer states with a universal scaling behavior in the limit $a \to \pm\infty$ (Braaten & Hammer, 2006). The universal geometrical scaling factor for three identical bosons is given by $e^{\pi/s_0} = 22.7$ with $s_0 = 1.00624$ (Braaten & Hammer, 2006). This means that when an Efimov state exists at $E = 0$ for a particular scattering length a, the next Efimov state emerges at a scattering length which is a factor 22.7 larger. Furthermore, the binding energies scale with the universal factor $e^{2\pi/s_0} \approx 515$ at $a \to \pm\infty$. So the scaling factor fixes the relative energy between the trimer states. However, an additional parameter is necessary to determine the absolute energy and the position of the first Efimov trimer. This additional parameter is known as the three-body parameter κ_* (Braaten & Hammer, 2006). The energy of the nth Efimov trimer at $a \to \pm\infty$ is given by (Braaten & Hammer, 2006)

$$E_T^{(n)} = -e^{-2\pi n/s_0}\frac{\hbar^2\kappa_*^2}{m}. \tag{2.2}$$

The binding energies at finite scattering length depend on both a and κ_*.

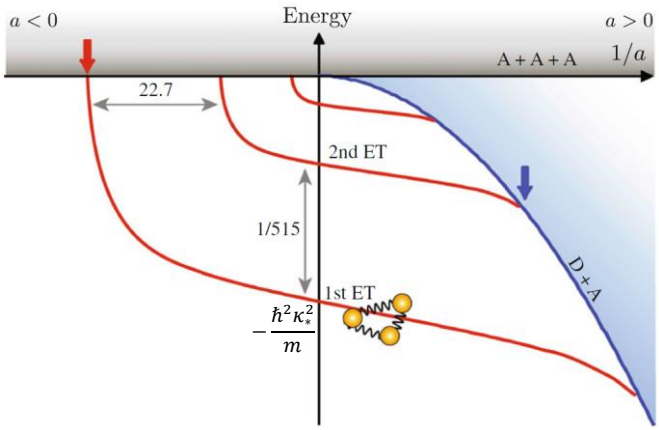

Fig. 2.1. Plot of the binding energy of the weakly bound Efimov trimer states (ET) as a function of the inverse two-body scattering length $1/a$ (Ferlaino et al., 2011). Only three Efimov states are depicted. Scattering continuum states for three atoms exist for $E > 0$, whereas the bound states occur for $E < 0$. Note that dimer states do not exist for negative scattering lengths. The deepest illustrated trimer state has a bound state energy $E = -\hbar^2\kappa_*^2/m$ at $a \to \pm\infty$. The scattering length at zero energy of this trimer state is indicated by the red arrow and it is called $a_0^{(-)}$.

As indicated above, the parameter κ_* could be used to determine the absolute energy and the position of the first Efimov trimer. However, another three-body parameter, namely $a_0^{(-)}$, is easier to measure in experiments. The parameter $a_0^{(-)}$ is the scattering length at zero energy of the same trimer state to which κ_* belongs. In Fig. 2.1 it is indicated by the red arrow. The three-body parameter is necessary because it bounds the ladder of Efimov states from below (Ferlaino et al., 2011). Finite range potentials always have a deepest lying Efimov state. The situation in which the bound states have an infinitely large binding energy is unphysical. It is only possible in a zero-range two-body interaction potential, which is known as the Thomas effect (Thomas, 1935). It is still an open issue how the three-body parameter is related to the short-range physics (Ferlaino et al., 2011), which includes both two-body and three-body contributions to the total interaction potential.

The three-body parameter $a_0^{(-)}$ corresponds to the deepest lying Efimov state for finite range potentials. The next trimer state will have a three-body parameter $a_1^{(-)}$. Finite range effects of the interaction potential can lead to non-universality in the scaling factor. Especially the first scaling factor $a_1^{(-)}/a_0^{(-)}$ will be influenced by the range of the potential because at lower scattering lengths the range of the potential will not be negligible.

Only the three-body parameter $a_0^{(-)}$ corresponding to the deepest lying Efimov state can be experimentally observed because of large atom losses as the scattering length increases (Schmidt, 2012). In these experiments the three-body parameter $a_0^{(-)}$ is determined by measuring the recombination length as function of the scattering length a. At $a = a_0^{(-)}$ a giant recombination loss is visible. This peak in the recombination length corresponds to a triatomic Efimov resonance (Kraemer et al., 2006), which means that three free atoms in the ultracold limit resonantly couple to a trimer. This resonance occurs at zero energy when the scattering length equals the scattering length of an Efimov state. So at $a = a_0^{(-)}$ a triatomic Efimov resonance is visible in the ultracold limit. Fig. 2.2 shows an experimental observation of the triatomic Efimov resonance. This experiment has also been conducted by the research group at the University of Innsbruck (Kraemer et al., 2006) who have provided the first signatures of a triatomic Efimov resonance.

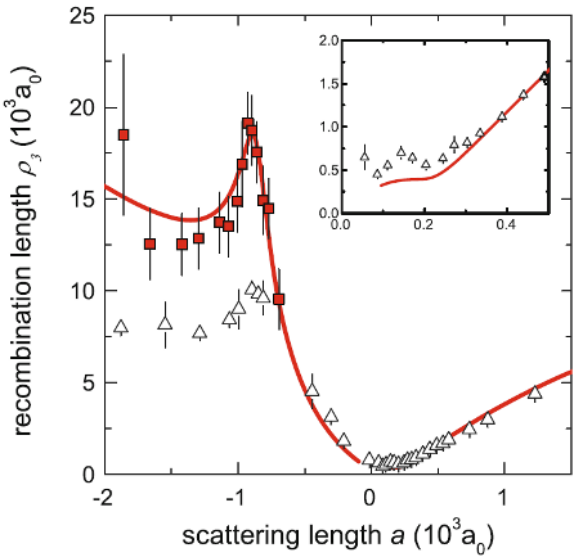

Fig. 2.2. Measurements of the recombination length ρ as function of the scattering length a (Ferlaino et al., 2011). The peak in the recombination length is the effect of triatomic Efimov resonance. Ultracold cesium atoms (squares: 10 nK; empty triangles: 200 nK) have been used in this experiment. The solid curve is analytically determined from effective field theory.

Recent experiments in ultracold atoms have revealed another unexpected universal characteristic of the Efimov spectrum, namely the universality of the three-body parameter when measured in units of an effective range (Horinouchi & Ueda, 2015). These experiments have shown that the three-body parameter falls within the universal window of $\kappa^* R_e = 0.44 - 0.52$ for deep potentials decaying faster than $1/r^6$ (Horinouchi & Ueda, 2015). Here R_e is the effective range which is defined by Eq. (4.49) in paragraph 4.9 of this report. The universality of the three-body parameter is an unexpected result because the three-body parameter encapsulates short-range details of the three-body physics (Horinouchi & Ueda, 2015).

Since the three-body parameter κ^* is universally related to the effective range of the two-body interaction potential, the three-body parameter $a_0^{(-)}$ which is more easily measured will also have a universal value. Experiments have demonstrated that $a_0^{(-)} \approx -9.8\, R_{vdW}$ for different atomic species, internal states and Feshbach resonances (Horinouchi & Ueda, 2015). Here R_{vdW} is the van der Waals length. Examples of experimental results are $a_0^{(-)} = -9.5(4)\, R_{vdW}$ (Berninger et al., 2011), $a_0^{(-)} = -9.7(7)\, R_{vdW}$ (Wild et al., 2012) and $a_0^{(-)} = -10.9(7)\, R_{vdW}$ (Roy et al., 2013). The van der Waals length represents the natural length scale which is associated with the van der Waals interaction (Ferlaino et al., 2011). It is defined as

$$R_{vdW} = \frac{1}{2}\left(\frac{mC_6}{\hbar^2}\right)^{1/4}, \qquad (2.3)$$

where the constant C_6 is related to the interaction potential. The long-range two-body interaction potential has a $-C_6/r^6$ tail which is governed by the van der Waals interaction (Ferlaino et al., 2011). The constant C_6 is a characteristic of the colliding particles.

.

3. Resonances in two-body collisions

Resonances play an important role in quantum scattering physics. They can lead to large increments in loss rates and peaks in elastic cross sections (Kokkelmans, 2014). Two resonance phenomena are particularly important for this report: the Feshbach resonance, which is used to experimentally observe the Efimov effect, and the potential resonance, which will be used in this report to simulate a Feshbach resonance. An important difference between both resonances is that the potential resonance cannot be tuned easily in general in contrast to the Feshbach resonance. The potential resonance is described in paragraph 3.1. Since Feshbach resonances are related to the coupling of different spin channels, paragraph 3.2 explains how a bound state in the energetically closed channel is formed during the collision. Paragraph 3.3 will link the Feshbach resonance with such bound states.

3.1 Potential resonance

A potential resonance is a pure s-wave phenomenon. It occurs in absence of an angular momentum barrier when a bound state or virtual state, which is an almost bound state, is close to the collision threshold of a single-channel interaction potential (Kokkelmans, 2014). The scattering length a is much larger than the range of the potential and characterizes the resonance. It can be written as

$$a = r_0 + a_P \tag{3.1}$$

in which r_0 is the non-resonant contribution to the scattering length and a_P is the resonant contribution which is related to the pole of the scattering matrix (Kokkelmans, 2014). This will be shown chapter 6 in case for a square well potential. The non-resonant contribution r_0 is on the order of the range of the interaction potential which is linked to the van der Waals range R_{vdW}.

3.2 Coupling of different spin channels

In an ultracold collision each atom is in a specific single-atom hyperfine state $|\alpha\rangle = |f\ m_f\rangle$ in which f is the effective spin of the atom with corresponding magnetic quantum number m_f (Kokkelmans, 2014). The effective spin is the sum of the electronic and nuclear spin. The energy ε_α of the hyperfine state $|\alpha\rangle$ depends on the magnetic field due to the hyperfine and Zeeman interactions. As a result, f is not a good quantum number at non-zero magnetic fields and multiple channels exist. When two atoms, which are in the hyperfine states $|\alpha\rangle$ and $|\beta\rangle$ with energy $E > \varepsilon_\alpha + \varepsilon_\beta$ (so they are in an open channel), collide, their hyperfine states may change and so does their potential energy. They may be trapped in a closed channel potential. This is possible when the total energy before the collision equals approximately the binding energy of the closed channel ($E \approx \varepsilon_Q$) and the transitions of the atoms $|\alpha\rangle \rightarrow |\alpha'\rangle$ and $|\beta\rangle \rightarrow |\beta'\rangle$ are allowed by the required selection rules. This is illustrated in figure 3.1. The scattering states of the closed channel are energetically forbidden because the energy E of the two-particle system is below the asymptotic energy $\varepsilon_{\alpha'} + \varepsilon_{\beta'}$ of the closed channel potential. The collision threshold energy ε_{thr} is defined as the asymptotic energy of the open channel potential, so $\varepsilon_{thr} = \varepsilon_\alpha + \varepsilon_\beta$.

Bound states in an energetically closed channel potential are discrete, whereas the scattering states form a continuum with kinetic energy $\frac{\hbar^2 k^2}{2\mu} = E - \varepsilon_{thr}$ (Kokkelmans, 2014). Here μ is the reduced mass of the two-particle system. In case of two identical bosons $\mu = \frac{1}{2} m$ with m the mass of a single boson.

If there is only one open channel, the ingoing channel is also the outgoing channel. This is called an on-shell scattering process because it is elastic. However, if there is more than one open channel, the collision threshold energy ε_{thr} of the ingoing channel does not have to be the same as ε_{thr} of the outgoing channel. The scattering process can be inelastic and the scattering process is called off-shell.

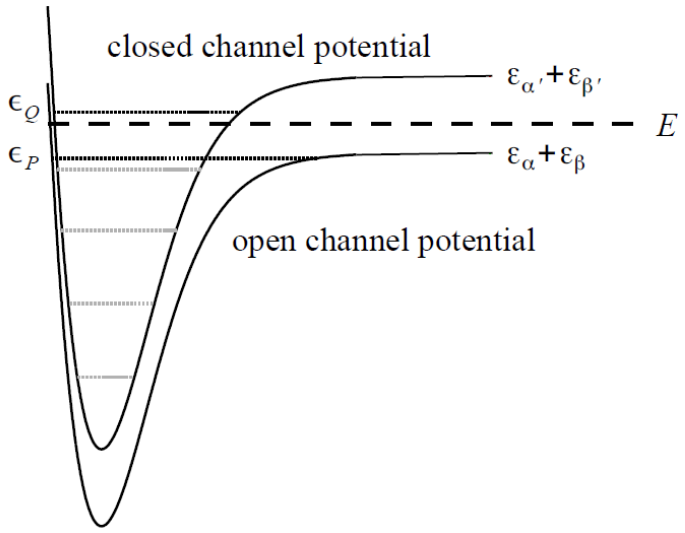

Fig. 3.1. Schematic representation of two coupled channels potentials (Kokkelmans, 2014). During the collision the two atoms with energy E may undergo the transitions $|\alpha\rangle \rightarrow |\alpha'\rangle$ and $|\beta\rangle \rightarrow |\beta'\rangle$. When this happens, the two atoms are trapped in the closed channel potential. In other words, a bound state has been formed.

3.3 Feshbach resonance

A Feshbach resonance (Feshbach, 1958) requires both an open channel and an energetically closed channel that is weakly coupled to the open channel (Braaten & Hammer, 2006). Since the channels correspond to different spin configurations of the atomic pair, the internal state energies can be tuned via external magnetic fields (Kokkelmans, 2014). After all, the energy of the hyperfine states depends on the magnetic field due to the hyperfine and Zeeman interactions. At resonance the total energy before the collision equals the binding energy of the closed channel which is shifted. As a result, the scattering of the particles in the open channel is enhanced (Braaten & Hammer, 2006). This is called a Feshbach resonance. The scattering length of a narrow Feshbach resonance is given by

$$a = a_{bg}\left(1 - \frac{\Delta B}{B - B_0}\right). \tag{3.2}$$

Here is a_{bg} the background scattering length which results from the background collision in the open channel, B_0 is the magnetic field of resonance and ΔB controls the width of the resonance (Kokkelmans, 2014) as is illustrated in Fig. 3.2. The scattering length diverges when $B = B_0$.

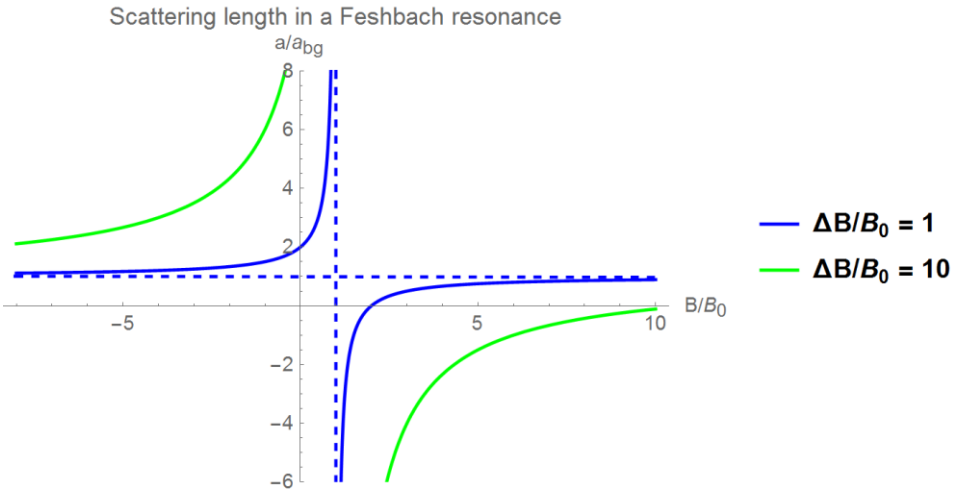

Fig. 3.2. Two-body scattering length a as function of the magnetic field B. The scattering length diverges for $B = B_0$. The width of the resonance is determined by ΔB.

4. Two-body scattering theory

In this chapter the theory of two-body scattering processes is given. Firstly, the Hamiltonian in two-particle systems is analyzed. It is shown that the two-body problem can be reduced to an equivalent one-body problem. Furthermore, the Lippmann-Schwinger equation is derived and the definitions of the scattering and transition operators are given. These operators can be used to calculate the S- and T-matrices. Moreover, the equation to calculate the off-shell wave function is given. This off-shell wave function is necessary for the calculation of the two-body off-shell T-matrix. Finally, partial wave analysis for on-shell scattering processes is carried out and the results are evaluated in the ultracold limit.

4.1 Two-particle systems

The state of a two-particle system Ψ is a function of the time and the position coordinates of particle one ($\boldsymbol{r_1}$) and particle two ($\boldsymbol{r_2}$). It satisfies the Schrödinger equation with Hamiltonian

$$H = -\frac{\hbar^2}{2m_1}\nabla_1^2 - \frac{\hbar^2}{2m_2}\nabla_2^2 + V(\boldsymbol{r}_1, \boldsymbol{r}_2, t). \tag{4.1}$$

If the potential V is time-independent, the eigenfunctions of the Schrödinger equation are separable and are given by

$$\Psi(\boldsymbol{r}_1, \boldsymbol{r}_2, t) = \psi(\boldsymbol{r}_1, \boldsymbol{r}_2)e^{-\frac{iEt}{\hbar}}. \tag{4.2}$$

Here E is the total energy of the system. The spatial wave function ψ satisfies the time-independent Schrödinger equation with the Hamiltonian of Eq. (4.1). If the interaction potential depends only on the relative position $\boldsymbol{r} = \boldsymbol{r}_1 - \boldsymbol{r}_2$ between the two particles, the Hamiltonian can be written as

$$H = -\frac{\hbar^2}{2(m_1+m_2)}\nabla_R^2 - \frac{\hbar^2}{2\mu}\nabla_r^2 + V(\boldsymbol{r}), \tag{4.3}$$

where $\boldsymbol{R} = \frac{m_1\boldsymbol{r}_1+m_2\boldsymbol{r}_2}{m_1+m_2}$ is the center of mass coordinate and $\mu = \frac{m_1m_2}{m_1+m_2}$ is the reduced mass. By separation of variables, $\psi(\boldsymbol{R}, \boldsymbol{r}) = \psi_R(\boldsymbol{R})\psi_r(\boldsymbol{r})$, the time-independent Schrödinger equation is given by

$$H_{cm}\psi_R = -\frac{\hbar^2}{2(m_1+m_2)}\nabla_R^2\psi_R = E_R\psi_R \text{ and} \tag{4.4}$$

$$H_{rel}\psi_r = -\frac{\hbar^2}{2\mu}\nabla_r^2\psi_r + V(\boldsymbol{r})\psi_r = E_r\psi_r. \tag{4.5}$$

The total energy is given by $E = E_R + E_r$. This result is proven in (Griffiths, 2014). This is an important result because it reduces the two-body problem to an equivalent one-body problem. After all, the relative motion is the same as if we had a single particle with reduced mass subject to the potential V (Griffiths, 2014).

4.2 Lippmann-Schwinger equation

For time-independent scattering processes the Hamiltonian can written as $H = H_0 + V$ where the kinetic-energy operator is given by $H_0 = \boldsymbol{p}^2/2m$. The state $|\phi\rangle$ is defined to be a plane-wave state or a free-spherical wave state and it is an eigenfunction of H_0 with eigenvalue E:

$$H_0|\phi\rangle = E|\phi\rangle. \tag{4.6}$$

Furthermore, the state $|\psi\rangle$ is an eigenfunction of H with the same eigenvalue E:

$$(H_0 + V)|\psi\rangle = E|\psi\rangle. \tag{4.7}$$

Combining Eq. (4.6) and Eq. (4.7) gives

$$|\psi\rangle = \frac{1}{E-H_0} V|\psi\rangle + |\phi\rangle. \tag{4.8}$$

However, the operator $\frac{1}{E-H_0}$ has a singular nature. Therefore the energy E is made slightly complex (Sakurai, 1994). The resulting equation is called the Lippmann-Schwinger equation and it is given by

$$|\psi^{(\pm)}\rangle = \frac{1}{E-H_0\pm i\epsilon} V|\psi^{(\pm)}\rangle + |\phi\rangle. \tag{4.9}$$

Here $\langle \boldsymbol{x}|\psi^{(+)}\rangle$ is the wave function with an outgoing spherical wave boundary condition and $\langle \boldsymbol{x}|\psi^{(-)}\rangle$ is the wave function with an ingoing spherical wave boundary condition. The inhomogeneous term $|\phi\rangle$ disappears when bound states are considered (i.e. $E < 0$).

4.3 Scattering operator

The time-dependent Schrödinger equation which is given by

$$i\hbar \frac{d}{dt}|\psi_t\rangle = H|\psi_t\rangle \tag{4.10}$$

has the general solution $|\psi_t\rangle = e^{-\frac{iHt}{\hbar}}|\psi\rangle$. Here $e^{-\frac{iHt}{\hbar}}$ is the evolution operator and $|\psi\rangle$is any vector in the appropriate Hilbert space (Taylor, 1972). For every scattering state $|\psi\rangle$ the orbit is given by $e^{-\frac{iHt}{\hbar}}|\psi\rangle$ and the in- and out-asymptotes are given by (Taylor, 1972)

$$\begin{cases} e^{-\frac{iHt}{\hbar}}|\psi\rangle \to e^{-\frac{iH_0t}{\hbar}}|\psi_{in}\rangle \; for\; t \to -\infty \\ e^{-\frac{iHt}{\hbar}}|\psi\rangle \to e^{-\frac{iH_0t}{\hbar}}|\psi_{out}\rangle \; for\; t \to \infty \end{cases}. \tag{4.11}$$

The Møller wave operators are defined as the limits (Taylor, 1972)

$$\Omega_{\pm} = \lim_{t\to\mp\infty} e^{iHt/\hbar}e^{-iH_0t/\hbar}. \tag{4.12}$$

When these operators act on any vector in the appropriate Hilbert space, they give the actual state at $t = 0$ that would evolve from (or to) the asymptote represented by that vector (labeled $|\psi_{in}\rangle$ or $|\psi_{out}\rangle$) (Taylor, 1972). So Eq. (4.11) and Eq. (4.12) give

$$|\psi\rangle = \Omega_+|\psi_{in}\rangle = \Omega_-|\psi_{out}\rangle. \tag{4.13}$$

Since the Møller wave operators are isometric (Taylor, 1972), Eq. (4.13) can be written as

$$|\psi_{out}\rangle = \Omega_-^\dagger\Omega_+|\psi_{in}\rangle = S|\psi_{in}\rangle. \tag{4.14}$$

Here the scattering operator S is defined as

$$S = \Omega_-^\dagger\Omega_+. \tag{4.15}$$

The scattering operator is useful because it gives $|\psi_{out}\rangle$ directly in terms of $|\psi_{in}\rangle$. These states, the asymptotic free motion, are observable in practice. Therefore the unitary operator S gives all information of experimental interest (Taylor, 1972). The scattering operator of two-particle scattering

is the same as the one-particle S operator in the center-of-mass reference frame. So the S operator should be computed from the Hamiltonian H_{rel} which is given in Eq. (4.5) (Taylor, 1972).

4.4 Transition operator

The transition operator T is defined such that (Sakurai, 1994)

$$V|\psi^{(+)}\rangle = T|\phi\rangle. \tag{4.16}$$

Combining this equation with the Lippmann-Schwinger equation (Eq. (4.9)) gives

$$T|\phi\rangle = V\frac{1}{E-H_0+i\epsilon}\,T|\phi\rangle + V|\phi\rangle. \tag{4.17}$$

So the transition operator satisfies the following equation:

$$T = V\frac{1}{E-H_0+i\epsilon}\,T + V = VG^0(z)\,T + V. \tag{4.18}$$

Here $G^0(z) = \frac{1}{z-H_0}$ is the Green's operator and $z = E + i\epsilon$ is the complex energy.

4.5 S-matrix and T-matrix

The scattering matrix (S-matrix) is given by $\langle \boldsymbol{k}'|S|\boldsymbol{k}\rangle$. It is nonzero as long as the plane-wave states $|\boldsymbol{k}\rangle$ and $|\boldsymbol{k}'\rangle$ have the same energy, so $|\boldsymbol{k}'| = |\boldsymbol{k}|$ (Taylor, 1972). So the S-matrix conserves energy. The S-matrix is related to the probability that a particle that enters the collision with in-asymptote $|\boldsymbol{k}\rangle$ is observed to leave with out-asymptote $|\boldsymbol{k}'\rangle$ (Taylor, 1972). This probability is given by

$$p(\boldsymbol{k}\to\boldsymbol{k}') = |\langle \boldsymbol{k}'|S|\boldsymbol{k}\rangle|^2. \tag{4.19}$$

This equation also holds for spherical wave states instead of plane-wave states. The off-shell T-matrix is given by $\langle \boldsymbol{k}'|T(z)|\boldsymbol{k}\rangle$ and is defined for all $\boldsymbol{k}'$, $\boldsymbol{k}$ and z. It reduces to the on-shell T-matrix $\langle \boldsymbol{k}'|T|\boldsymbol{k}\rangle_{on}$ in the limit $|\boldsymbol{k}'|\to|\boldsymbol{k}|$ and $z\to\hbar^2k^2/2m$ and to the half-off-shell T-matrix $\langle \boldsymbol{k}'|T|\boldsymbol{k}\rangle_{half-off}$ in the limit $z\to\hbar^2k^2/2m$. The S-matrix is related to the on-shell T-matrix $\langle \boldsymbol{k}'|T|\boldsymbol{k}\rangle_{on}$ by (Taylor, 1972)

$$\langle \boldsymbol{k}'|S|\boldsymbol{k}\rangle = \delta^{(3)}(\boldsymbol{k}-\boldsymbol{k}') - 2\pi i\,\delta(E_{k'}-E_k)\langle \boldsymbol{k}'|T|\boldsymbol{k}\rangle_{on}. \tag{4.20}$$

So the on-shell T-matrix determines the S-matrix. However, not only the on-shell T-matrix is relevant in scattering experiments. Off-shell two-body T-matrices are relevant in multi-particle scattering processes. The off-shell T-matrix can be calculated from Eq. (4.17) as follows

$$\begin{aligned}\langle \boldsymbol{k}'|T(z)|\boldsymbol{k}\rangle &= \langle \boldsymbol{k}'|V|\boldsymbol{k}\rangle + \langle \boldsymbol{k}'|VG^0(z)T|\boldsymbol{k}\rangle \\ &= \langle \boldsymbol{k}'|V|\boldsymbol{k}\rangle + \int \frac{\langle \boldsymbol{k}'|V|\boldsymbol{k}''\rangle}{z-E_{k''}}\,\langle \boldsymbol{k}''|T(z)|\boldsymbol{k}\rangle\, d^3\boldsymbol{k}''.\end{aligned} \tag{4.21}$$

This equation shows that if one wants to calculate the on-shell T-matrix via the Lippmann-Schwinger equation at least the half-off-shell T-matrix is involved (Taylor, 1972). After all, if one sets $z\to\hbar^2k^2/2m$ and $k'\to k$, there is still an integral of which the integrand includes the half-off-shell T-matrix $\langle \boldsymbol{k}''|T(\hbar^2k^2/2m)|\boldsymbol{k}\rangle$. Furthermore, Eq. (4.9) and Eq. (4.16) give

$$\langle \boldsymbol{x}|\psi^{(+)}\rangle = \langle \boldsymbol{x}|\boldsymbol{k}\rangle + \int \frac{\langle \boldsymbol{x}|\boldsymbol{k}''\rangle}{z-E_{k''}}\,\langle \boldsymbol{k}''|T(z)|\boldsymbol{k}\rangle\, d^3\boldsymbol{k}''. \tag{4.22}$$

So the wave function can be calculated for all values of $\boldsymbol{x}$ when at least the half-off-shell T-matrix $\langle \boldsymbol{k}'|T|\boldsymbol{k}\rangle_{half-off}$ is known for all values $\boldsymbol{k}'$ (Landau, 1996). The on-shell T-matrix determines only

the scattering amplitude and thus the asymptotic wave function ($r \to \infty$) (Landau, 1996). Using Eq. (4.16) The off-shell T-matrix can also be expressed as

$$\langle \boldsymbol{k}'|T|\boldsymbol{k}\rangle = \langle \boldsymbol{k}'|V|\psi^{(+)}\rangle = \iint \langle \boldsymbol{k}'|\boldsymbol{x}'\rangle\langle \boldsymbol{x}'|V|\boldsymbol{x}''\rangle\langle \boldsymbol{x}''|\psi^{(+)}\rangle \, d^3\boldsymbol{x}' d^3\boldsymbol{x}''. \tag{4.23}$$

Note that the $|\psi^{(+)}\rangle$ is an off-shell wave function that depends on a complex energy z and a momentum k. Next paragraph will show how this off-shell wave function should be calculated.

The potential V is local if it can be written as (Sakurai, 1994)

$$\langle \boldsymbol{x}'|V|\boldsymbol{x}''\rangle = V(\boldsymbol{x}')\delta^{(3)}(\boldsymbol{x}' - \boldsymbol{x}''). \tag{4.24}$$

In this report the considered potentials are functions only of the position operator, so they are all local. In case of a local potential Eq. (4.23) can be written as

$$\langle \boldsymbol{k}'|T|\boldsymbol{k}\rangle = \int \langle \boldsymbol{k}'|\boldsymbol{x}'\rangle V(\boldsymbol{x}')\langle \boldsymbol{x}'|\psi^{(+)}\rangle \, d^3\boldsymbol{x}'. \tag{4.25}$$

Note that $\boldsymbol{x}'$ is just an integration variable. This vector should not be confused with the momentum vector $\boldsymbol{k}'$.

4.6 Off-shell wave function

Three-body collisions require knowledge of the fully off-shell two-body T-matrix over the entire momentum space (Cheng et al., 1990). In order to calculate the two-body off-shell T-matrix the off-shell wave function should be determined. This wave function is calculated from the off-shell analog of the Lippmann-Schwinger equation. First, we consider the Lippmann-Schwinger equation for the Møller wave operators. It is given by (Levine, 1969)

$$(z - H)\Omega(z) = z - H_0 \tag{4.26}$$

where the complex variable z is the complex energy. The real part of z equals the energy E. The operator $\Omega(z)$ is related to the Møller wave operator Ω_+ by (Levine, 1969)

$$\Omega_+ = \int \Omega(E^+)\delta(E - H_0)dE \tag{4.27}$$

where $E^+ = E + i\epsilon$ with ϵ real and positive and the limit $\epsilon \to 0$ is understood at the final stage. The operator $\Omega(z)$ satisfies the equation (Levine, 1969)

$$|\psi\rangle = \Omega(E^+)|\psi_{in}\rangle. \tag{4.28}$$

Next, we take matrix elements of both sides of Eq. (4.26) with respect to $|\boldsymbol{x}\rangle$ and $|\boldsymbol{k}\rangle$ where $\boldsymbol{k}$ can be off the energy shell. So, the energy E need not to be equal to $\hbar^2k^2/2m$. The resulting equation is (Cheng et al., 1990)

$$\left(z + \frac{\hbar^2}{2m}\nabla^2 - V(\boldsymbol{x})\right)\psi_{\boldsymbol{k}}(\boldsymbol{x}, z) = \frac{1}{(2\pi)^{\frac{3}{2}}}\frac{\sqrt{4\pi km}}{\hbar}\left(z - \frac{\hbar^2k^2}{2m}\right)e^{i\boldsymbol{k}\cdot\boldsymbol{x}}. \tag{4.29}$$

The off-shell wave function is $\psi_{\boldsymbol{k}}(\boldsymbol{x}, z) = \langle \boldsymbol{x}|\Omega(z)|\boldsymbol{k}\rangle$ which follows from Eq. (4.28). After all, $|\boldsymbol{k}\rangle$ is the incoming plane-wave state. Note that the energy normalization condition is used in Eq. (4.29). Since s-wave scattering dominates at low collision energies which will be shown in section 4.8, it is assumed that the wave function $\psi_{\boldsymbol{k}}(\boldsymbol{x}, z)$ does not depend on θ and ϕ, but only on the relative distance r between the particles. This means that the angle between $\boldsymbol{k}$ and $\boldsymbol{k}'$ is assumed to be zero. In this case the wave function can be written as $\psi_{\boldsymbol{k}}(\boldsymbol{x}, z) = u(r)/r$. Now the off-shell Schrödinger equation can written as

$$\frac{d^2u}{dr^2} = -\big(z - V(r)\big)\frac{2m}{\hbar}u(r) + \frac{1}{(2\pi)^{\frac{3}{2}}}\frac{\sqrt{4\pi km}}{\hbar}\Big(\frac{2mz}{\hbar^2 k} - k\Big)\sin kr. \tag{4.30}$$

4.7 Spherical-wave states

Spherical-wave states are convenient to use when one is considering scattering by a spherically symmetric potential. In section 4.2 it was stated that the state $|\phi\rangle$ is a plane-wave state or a free-spherical wave state and that it is an eigenfunction of H_0 with eigenvalue E. Since the free-particle Hamiltonian H_0 also commutes with angular momentum operators $\boldsymbol{L}^2$ and L_z, it is possible to consider a simultaneous eigenfunction of H_0, $\boldsymbol{L}^2$ and L_z. If the spin angular momentum is ignored, this state is denoted by $|E, l, m\rangle$. Here l is the azimuthal quantum number and m is the magnetic quantum number. The state $|E, l, m\rangle$ is called a spherical-wave state (Sakurai, 1994). The normalization convention for these spherical-wave states is given by

$$\langle E', l', m'|E, l, m\rangle = \delta_{ll'}\delta_{mm'}\delta(E - E'). \tag{4.31}$$

The wavenumber normalization convention for the plane-wave states $|\boldsymbol{k}\rangle$ is given by

$$\langle \boldsymbol{k}|\boldsymbol{k}'\rangle = \delta^{(3)}(\boldsymbol{k} - \boldsymbol{k}'). \tag{4.32}$$

According to (Sakurai, 1994) the plane-wave state $|\boldsymbol{k}\rangle$ can be expanded in the spherical-wave basis:

$$|\boldsymbol{k}\rangle = \sum_{l=0}^{\infty}\sum_{m=-l}^{l}|E, l, m\rangle|_{E=\frac{\hbar^2k^2}{2m}}\left(\frac{\hbar}{\sqrt{mk}}Y_l^{m*}\big(\widehat{\boldsymbol{k}}\big)\right) \tag{4.33}$$

where the normalization condition of Eq. (4.32) has been used. From Eq. (4.33) it follows that

$$\langle \boldsymbol{k}|E, l, m\rangle = \frac{\hbar}{\sqrt{mk}}\delta\left(\frac{\hbar^2k^2}{2m} - E\right)Y_l^m\big(\widehat{\boldsymbol{k}}\big). \tag{4.34}$$

Furthermore, it can be shown (Sakurai, 1994) that

$$\langle \boldsymbol{x}|E, l, m\rangle = \frac{i^l}{\hbar}\sqrt{\frac{2mk}{\pi}}j_l(kr)Y_l^m(\hat{\boldsymbol{r}}) \tag{4.35}$$

where $j_l(kr)$ is the spherical Bessel function of order l. The T-matrix can also be expressed in the spherical-wave basis as

$$\langle E', l', m'|T|E, l, m\rangle = T_l(E)\delta_{ll'}\delta_{mm'}. \tag{4.36}$$

Here the Wigner-Eckart theorem has been used (Sakurai, 1994) to show that the T-matrix is diagonal both in l and in m. The wavenumber normalized T-matrix is related to the partial-wave T-matrix elements $T_l(E)$ by

$$\langle \boldsymbol{k}'|T|\boldsymbol{k}\rangle = \frac{\hbar^2}{km}\sum_l\sum_m T_l(E)|_{E=\hbar^2k^2/2m}\,Y_l^m\big(\widehat{\boldsymbol{k}}'\big)Y_l^{m*}\big(\widehat{\boldsymbol{k}}\big) \tag{4.37}$$

Similarly, the S-matrix is also diagonal in the angular-momentum representation. So it can be written as (Taylor, 1972)

$$\langle E', l', m'|S|E, l, m\rangle = S_l(E)\delta_{ll'}\delta_{mm'}\delta(E' - E). \tag{4.38}$$

Thus the dimensionless numbers $S_l(E)$ are the eigenvalues of the scattering operator belonging to the eigenvector $|E, l, m\rangle$ (Taylor, 1972). Since the scattering operator is unitary, the absolute value of $S_l(E)$ is one and it can be written as

$$S_l(E) = e^{2i\delta_l(E)}. \tag{4.39}$$

where the real number $\delta_l(E)$ is the phase shift.

4.8 Partial wave analysis for on-shell scattering

In on-shell quantum scattering theory an incident plane wave with momentum $\hbar\boldsymbol{k}$ (for example $\boldsymbol{k} = k\hat{\boldsymbol{z}}$) is considered which encounters a scattering potential V which produces an outgoing spherical wave with wave number k. So the solutions will have the general form

$$\langle \boldsymbol{x}|\psi^{(+)}\rangle \to \frac{1}{(2\pi)^{\frac{3}{2}}}\left(e^{i\boldsymbol{k}\cdot\boldsymbol{x}} + \frac{e^{ikr}}{r} f(\boldsymbol{k}', \boldsymbol{k})\right) for\ r \to \infty. \tag{4.40}$$

Here $f(\boldsymbol{k}', \boldsymbol{k})$ is the scattering amplitude. The outgoing wavenumber is directed in the radial direction. It is given by $\boldsymbol{k}' = k\hat{\boldsymbol{r}}$ where the scattering process is assumed to be on-shell. In (Sakurai, 1994) it is derived that

$$\begin{aligned} f(\boldsymbol{k}', \boldsymbol{k}) &= -\frac{1}{4\pi}\frac{2m}{\hbar^2}(2\pi)^3 \langle \boldsymbol{k}'|T|\boldsymbol{k}\rangle_{on} = -\frac{1}{4\pi}\frac{2m}{\hbar^2}(2\pi)^3 \langle \boldsymbol{k}'|V|\psi^{(+)}\rangle \\ &= -\frac{1}{4\pi}\frac{2m}{\hbar^2}(2\pi)^3 \int d^3x' \frac{e^{-i\boldsymbol{k}'\cdot\boldsymbol{x}'}}{(2\pi)^{\frac{3}{2}}}\ V(\boldsymbol{x}')\langle \boldsymbol{x}'|\psi^{(+)}\rangle. \end{aligned} \tag{4.41}$$

In the derivation of Eq. (4.41) it is assumed that the potential V is local. The normalization condition of Eq. (4.32) was used in Eq. (4.40) and Eq. (4.41). Furthermore, we will assume that the potential is spherically symmetric, so that (Sakurai, 1994)

$$f(\boldsymbol{k}', \boldsymbol{k}) = f(\theta) = \sum_{l=0}^{\infty}(2l+1) f_l(k) P_l(\cos\theta). \tag{4.42}$$

Here $P_l(\cos\theta)$ are Legendre polynomials, l is the orbital angular momentum quantum number of the scattered particle and $f_l(k)$ is called the lth partial wave amplitude. If the incident particle is traveling in the positive z-direction, Eq. (4.40) can be written as (Sakurai, 1994)

$$\begin{aligned} &\langle \boldsymbol{x}|\psi^{(+)}\rangle \to \frac{1}{(2\pi)^{\frac{3}{2}}}\left(e^{ikz} + \frac{e^{ikr}}{r} f(\theta)\right) for\ large\ r. \\ &= \frac{1}{(2\pi)^{\frac{3}{2}}}\sum_l (2l+1)\frac{P_l(\cos\theta)}{2ik}\left(\left(1 + 2ikf_l(k)\right)\frac{e^{ikr}}{r} - \frac{e^{-i(kr-l\pi)}}{r}\right). \end{aligned} \tag{4.43}$$

Here Eq. (4.42) was used. Eq. (4.43) shows that the presence of the potential changes only the coefficient of the outgoing wave, $1 \to \left(1 + 2ikf_l(k)\right)$, whereas the ingoing wave is completely unaffected. So the partial-wave scattering matrix element $S_l(k)$ is given by

$$S_l(k) = e^{2i\delta_l(k)} = 1 + 2ikf_l(k). \tag{4.44}$$

Here $2\delta_l(k)$ is the phase change of the outgoing wave. Eq. (4.44) can also written as

$$f_l(k) = \frac{e^{2i\delta_l(k)} - 1}{2ik} = \frac{e^{i\delta_l(k)}\sin\delta_l(k)}{k} = \frac{1}{k\ \cot\delta_l - ik}. \tag{4.45}$$

4.9 Ultracold limit

At low energies scattering with a finite range potential is dominated by s-wave scattering (Sakurai, 1994). This corresponds to $l = 0$ and $m = 0$. Here a low energy means that the wavelength is comparable to or larger than the range of the potential. The effective potential which is given by

$$V_{eff}(r) = V(r) + \frac{\hbar^2}{2m}\frac{l(l+1)}{r^2}. \quad (4.46)$$

shows that a centrifugal barrier exists for $l \neq 0$. Classically, the domination of s-wave scattering can be understood by considering that the particle cannot penetrate the centrifugal barrier and thus it does not notice the potential $V(r)$ inside. However, in quantum mechanics a shape resonance might occur when the potential is strong enough to accommodate $l \neq 0$ bound states near $E \cong 0$ (Sakurai, 1994). If we assume that there is no shape resonance, it can be shown (Sakurai, 1994) that the phase shift goes to zero as

$$\delta_l \sim k^{2l+1} \quad (4.47)$$

for small k. This is known as the threshold behavior (Sakurai, 1994). So s-wave scattering usually dominates at low collision energies. Eq. (4.42) simplifies to

$$f(\boldsymbol{k}', \boldsymbol{k}) = f_0(k) = \frac{1}{k\cot\delta_0 - ik} \quad . \quad (4.48)$$

The s-wave scattering length a and the effective range R_e are defined by the effective range expansion

$$k\cot\delta_0 = -\frac{1}{a} + \frac{R_e}{2}k^2 + O(k^4). \quad (4.49)$$

The scattering length a governs low energy scattering, while the effective range R_e tells when the energy is low enough to be governed only by a (Taylor, 1972).

4.10 Normalization

Until now we have made use of the wavenumber normalization condition given by Eq. (4.32). From now on we will use the energy normalization condition in this report which is given by

$$\int_V \psi^*(\vec{r}, E')\psi(\vec{r}, E)d^3\vec{r} = \delta(E - E'), \quad (4.50)$$

so that the T-matrix $\langle \boldsymbol{k}'|T(z)|\boldsymbol{k}\rangle$ is dimensionless. When there is no dependence on either θ or ϕ and the energy is given by $E = \hbar^2k^2/2m$, it can be proved that

$$\delta^{(3)}(\boldsymbol{k} - \boldsymbol{k}') = \frac{1}{4\pi k^2}\delta(k - k') = \frac{\hbar^2}{4\pi mk}\delta(E - E'). \quad (4.51)$$

So for example Eq. (4.40) can be rewritten as

$$\langle \boldsymbol{x}'|\psi^{(+)}\rangle \rightarrow \sqrt{\frac{4\pi mk}{\hbar^2}}\frac{1}{(2\pi)^{\frac{3}{2}}}\left(e^{i\boldsymbol{k}\cdot\boldsymbol{x}} + \frac{e^{ikr}}{r}f(\boldsymbol{k}', \boldsymbol{k})\right) for\ r \rightarrow \infty. \quad (4.52)$$

5. Three-body scattering theory

In 1957 Skorniakov and Ter-Martirosian derived an equation for the three-body scattering problem (Skorniakov & Ter-Martirosian, 1957). In their derivation they made use of Jacobi coordinates, which are firstly explained. Next, the simplified STM-equation for low energy atom-dimer scattering is given, which is an integral equation for a function of a single variable.

5.1 Jacobi coordinates

A set of Jacobi coordinates consists of two vectors: the separation vector $\boldsymbol{\rho}_{23}$ between a pair of atoms and the separation vector $\boldsymbol{\rho}_1$ of the third atom from the center-of-mass of the pair (Braaten & Hammer, 2006). For three identical bosons these vectors are given by (Skorniakov & Ter-Martirosian, 1957)

$$\begin{cases} \boldsymbol{\rho}_{23} = \boldsymbol{r}_2 - \boldsymbol{r}_3 \\ \boldsymbol{\rho}_1 = \boldsymbol{r}_1 - \frac{1}{2}(\boldsymbol{r}_2 + \boldsymbol{r}_3) \end{cases}. \tag{5.1}$$

Here we could also have introduced the two pairs of vectors $\boldsymbol{\rho}_{12}$, $\boldsymbol{\rho}_3$ and $\boldsymbol{\rho}_{31}$, $\boldsymbol{\rho}_2$ in analogy to $\boldsymbol{\rho}_{23}$, $\boldsymbol{\rho}_1$. The vectors $\boldsymbol{r}_1$, $\boldsymbol{r}_2$ and $\boldsymbol{r}_3$ are the position coordinates of the three particles. By using Jacobi coordinates the Schrödinger equation for three identical bosons with mass m can be written as (Skorniakov & Ter-Martirosian, 1957)

$$\left(-\frac{\hbar^2}{m}\left(\nabla^2_{\boldsymbol{\rho}_{23}} + \frac{3}{4}\nabla^2_{\boldsymbol{\rho}_1}\right) - E\right)\psi(\boldsymbol{\rho}_{23}, \boldsymbol{\rho}_1) = -\big(V(\boldsymbol{\rho}_{23}) + V(\boldsymbol{\rho}_{12}) + V(\boldsymbol{\rho}_{31})\big)\psi(\boldsymbol{\rho}_{23}, \boldsymbol{\rho}_1). \tag{5.2}$$

Here an important property of the wave function for identical bosons has been used, namely the symmetry of the wave function relative to a permutation of particles. Eq. (5.2) can be written into integral form (Skorniakov & Ter-Martirosian, 1957). The result is the Skorniakov-Ter-Martirosian equation.

5.2 Skorniakov-Ter-Martirosian equation

In this section we consider s-wave scattering of a particle by a bound state of the other two. The particles are identical bosons with mass m. The dimer exists only for positive scattering lengths, $a > 0$, and negative energies. Its binding energy is given by $E = -\frac{\hbar^2}{ma^2}$. The Skorniakov-Ter-Martirosian equation describes the repeated scattering of an atom with a pair of atoms. Actually, the STM-equation is just a three-body Lippmann-Schwinger equation. However, since we consider the regime in which Efimov trimers may exist, i.e. $E < 0$, no inhomogeneous term will be present in this three-body equation in contrast to the Lippmann-Schwinger equation given by Eq. (4.9). The simplified STM-equation for low energy atom-dimer scattering, which can be used to find the trimer energy E, is given by (Levinsen, 2013)

$$T_3(k) = 2\int \frac{d^3p}{(2\pi)^3} \frac{T_2\left(\left|\boldsymbol{k}-\frac{\boldsymbol{p}}{2}\right|, \left|\boldsymbol{p}-\frac{\boldsymbol{k}}{2}\right|, E-\frac{3k^2}{4m}\right)}{E-k^2/m-p^2/m-\boldsymbol{k}\cdot\boldsymbol{p}/m} T_3(p). \tag{5.3}$$

Here $T_3(k)$ is the atom-dimer scattering T-matrix and $T_2(k', k, \hbar^2q^2/m)$ is the two-body T-matrix for atom-atom scattering in the center of mass frame with incoming momentum $\pm\boldsymbol{k}$ and outgoing momentum $\pm\boldsymbol{k}'$ and total energy $\frac{\hbar^2q^2}{2\mu_2} = \hbar^2q^2/m$ in which the reduced mass of the two-particle system $\mu_2 = \frac{1}{2}m$ has been used. Note that q can be either real, which results in positive energies, or purely imaginary to account for negative values of E. Furthermore, note that $\hbar$ has been set to unity in Eq. (5.3). The energy E of the three-particle system is $-\frac{3{q_3}^2}{4m}$. The two-body T-matrix in Eq. (5.3) should not be energy normalized, but it should satisfy the following momentum normalization condition:

$$\langle \boldsymbol{k}|\boldsymbol{k}'\rangle = (2\pi)^3\hbar^2\,\delta^{(3)}(\boldsymbol{k}-\boldsymbol{k}'). \qquad (5.4)$$

So the energy normalized two-body T-matrix should be multiplied with $\frac{2\pi^2}{\mu_2\sqrt{k\,k'}} = \frac{4\pi^2}{m\sqrt{k\,k'}}$ to obtain the momentum normalized T-matrix which should be substituted in Eq. (5.3). Note that μ_2 is the reduced mass of the two-particle system.

Although the total energy of the three-particle system is conserved, the two-body collisions can be inelastic. It is important to incorporate these inelastic collisions into Efimov physics. Therefore the two-body T-matrix in the STM-equation needs to be off-shell.

6. S-wave scattering by a finite square well potential

In this section s-wave scattering of a particle with mass *m* by a finite square well potential is analyzed. As was shown in section 4.1, this one-body problem is equivalent to the two-body scattering problem by considering the relative position between the two particles and by replacing the particle's mass *m* by the reduced mass. Moreover, the scattering length is calculated and the energy of the highest energy bound state is approximated. Furthermore, the S-matrix, on-shell T-matrix and half-off-shell T-matrix are calculated. Finally, the off-shell wave function is found. It is used to determine the off-shell two-body T-matrix.

Consider the three-dimensional square well potential which is given by

$$V = \begin{cases} -V_0 & for\ r \le R \\ 0 & for\ r > R \end{cases}. \tag{6.1}$$

In the low energy limit the angular momentum is zero, so $l = 0$ and the radial Schrödinger equation is given by

$$-\frac{\hbar^2}{2m}\frac{d^2u}{dr^2} = \big(E - V(r)\big)u(r). \tag{6.2}$$

Here the time-independent wave function $\psi(r,\theta,\phi) = R(r)Y_0^0(\theta,\phi) = \frac{R(r)}{\sqrt{4\,\pi}} = \frac{u(r)/r}{\sqrt{4\,\pi}}$.

6.1 S-wave scattering ($E > 0$)

Introducing the wave numbers $k = \sqrt{\frac{2mE}{\hbar^2}}$ and $K = \sqrt{\frac{2m(E+V_0)}{\hbar^2}}$ and solving Eq. (6.2) gives

$$u(r) = \begin{cases} A\ \sin Kr + B\cos Kr & for\ r \le R \\ F\sin(kr + \delta_0) & for\ r > R \end{cases}. \tag{6.3}$$

Using the boundary condition which states that the radial part $R(r) = u(r)/r$ of the wave function is finite at $r = 0$ gives $B = 0$. Furthermore, the boundary conditions at $r = R$ states that both the wave function and its derivative should be continuous at $r = R$. This gives

$$\begin{cases} A\ \sin KR = F\sin(kR + \delta_0) \\ AK\cos KR = Fk\cos(kR + \delta_0) \end{cases}', \tag{6.4}$$

which can be transformed into

$$\frac{1}{K}\tan KR = \frac{1}{k}\tan(kR + \delta_0). \tag{6.5}$$

Eq. (6.5) can be written as

$$\tan\delta_0 = \frac{k\ \tan KR - K\tan kR}{K + k\tan kR\tan KR}. \tag{6.6}$$

The scattering length a can be calculated from the phase shift using Eq. (4.49) which gives

$$a = -\lim_{k\to 0}\frac{1}{k}\tan\delta_0 = R\left(1 - \frac{\tan K_0R}{K_0R}\right). \tag{6.7}$$

So a is a function of the radius R and depth V_0 of the square well potential since K_0 is defined by $K_0 = \lim_{k\to 0} K = \sqrt{\frac{2mV_0}{\hbar^2}}$ in this low energy limit. Fig. 6.1 shows a graph of the scattering length versus K_0R. This figure shows that the scattering length diverges when $K_0R = \pi/2, 3\pi/2, 5\pi/2$, etc. Note that the width of these resonances decreases when the product K_0R increases. When a diverges, a bound state exists with energy $E = 0$. Since the energy of the scattered particle is slightly positive in low energy scattering, the resonance is a result of a state which is almost bound and such a state is called a 'virtual state' (Kokkelmans, 2014). Note that Eq. (6.7) has the same form as Eq. (3.1). The non-resonant contribution to the scattering length is the width of the square well ($r_0 = R$) and the resonant contribution is given by

$$a_p = -\frac{1}{K_0}\tan K_0 R. \tag{6.8}$$

The effective range can also be calculated from the phase shift by expanding $k\cot\delta_0$ in a Taylor series and comparing it with Eq. (4.49). The result is

$$R_e = 2R\left(1 - \frac{R}{a} + \frac{R^2}{3a^2}\right) \tag{6.9}$$

which is in agreement with (Kokkelmans, 2014) where the effective range of a potential resonance is given.

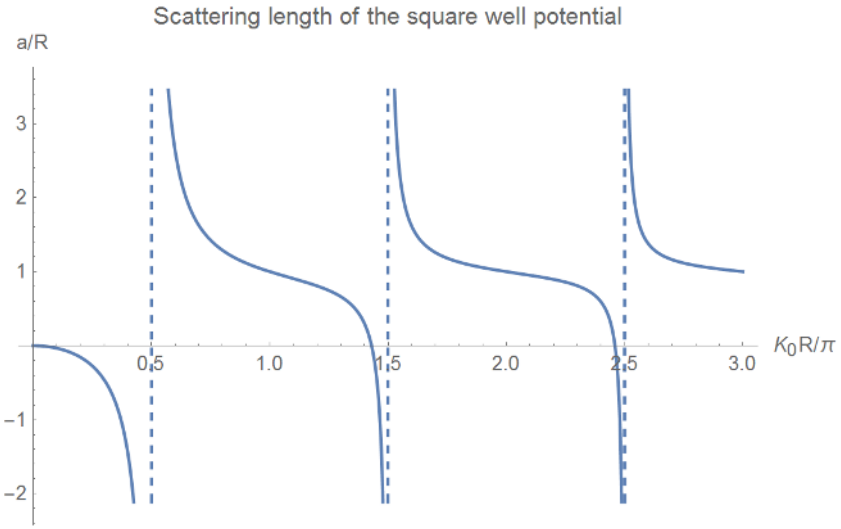

Fig. 6.1. Plot of a/R versus K_0R/π for scattering by the square well potential. The scattering length diverges when $K_0R = \pi/2, 3\pi/2, 5\pi/2$, etc.

It is easy to show that the scattering length a is nothing more than the intercept of the outside-wave function (Sakurai, 1994). This is illustrated in Fig. 6.2. The state with $K_0 = (\frac{5}{2}\pi - 0.05)$ is just unbound. Its scattering length is negative, whereas the state with $K_0R = (\frac{5}{2}\pi + 0.05)$ has a positive scattering length. The sign change resulting from increased attraction is related to the development of a bound state (Sakurai, 1994).

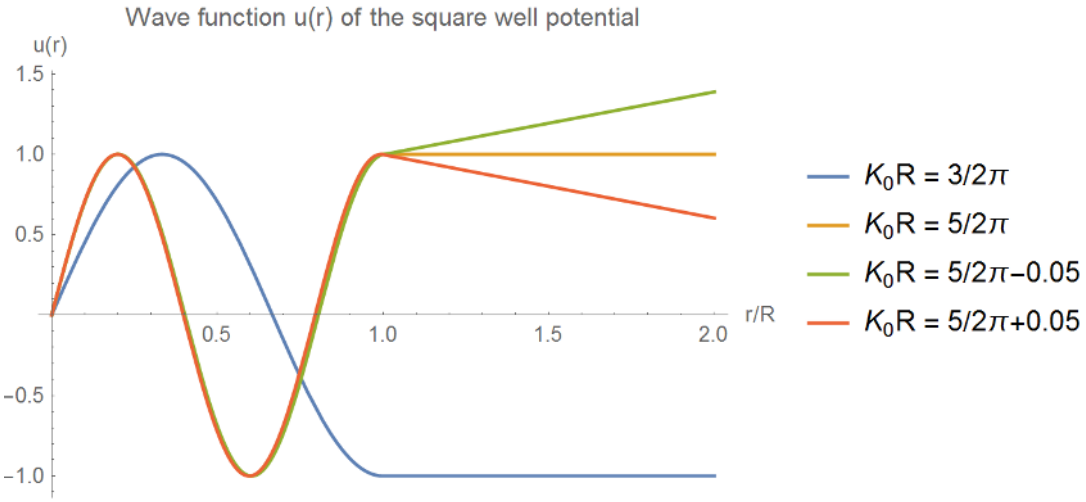

Fig. 6.2. Plot of u(r) versus r/R for scattering by the square well potential with $k \to 0$ and the constant A in Eq. (6.3) is chosen to be one. The outside-wave function does not intercept the x-axis for $K_0R = 3\pi/2$ and $K_0R = 5\pi/2$. The scattering length is negative for $K_0R = 5\pi/2 - 0.05$ and positive for $K_0R = 5\pi/2 + 0.05$. The sign change resulting from increased attraction is related to the development of a bound state (Sakurai, 1994).

6.2 Low energy bound states ($E < 0$)

Real bound states exist for $E < 0$. The solution to Eq. (6.2) is now given by

$$u(r) = \begin{cases} A\ \sin Kr + B\ \cos Kr & for\ r \le R \\ Ce^{-\kappa r} + De^{\kappa r} & for\ r > R \end{cases} \tag{6.10}$$

where $\kappa = \sqrt{\frac{2m|E|}{\hbar^2}}$ and $K = \sqrt{\frac{2m(E+V_0)}{\hbar^2}}$. Using the boundary condition which states that the radial part $R(r) = u(r)/r$ of the wave function is finite at $r = 0$ and at $r \to \infty$ gives $B = 0$ and $D = 0$. Continuity of the wave function and its derivative at $r = R$ gives

$$\begin{cases} A\ \sin KR = Ce^{-\kappa R} \\ AK\cos KR = -Cke^{-\kappa R}. \end{cases} \tag{6.11}$$

Eq. (6.11) gives

$$\frac{1}{K}\tan KR = -\frac{1}{\kappa}. \tag{6.12}$$

Now we consider the highest energy bound state and suppose that its energy is close to zero, so that $K = \sqrt{\frac{2mV_0}{\hbar^2}}$ approximately. Combining Eq. (6.12) and Eq. (6.7) gives

$$\kappa = \frac{1}{a-R} \approx \frac{1}{a} \tag{6.13}$$

if $R \ll a$ and the energy of the highest energy bound state is given by

$$E = -\frac{\hbar^2\kappa^2}{2m} \approx -\frac{\hbar^2}{2ma^2}. \tag{6.14}$$

6.3 S-matrix and on-shell T-matrix of the square well potential

The scattering matrix of the square well potential (abbreviated as S_{sw}) can be calculated using Eq. (4.44) and Eq. (6.6). The result is

$$S_{sw}(k) = e^{2i\delta_0(k)} = e^{-2ikR}\frac{1+i\frac{k}{K}\tan KR}{1-i\frac{k}{K}\tan KR}. \tag{6.15}$$

This shows that the S-matrix can be written as the product of a non-resonant scattering contribution, e^{-2ikR} , and a resonant scattering contribution that accounts for a pole at $k = -i\,K\cot KR = i\kappa \approx i/a_P$ in this low energy limit. The on-shell T-matrix can be calculated using Eq. (4.20) which results in

$$\begin{aligned} T_{sw,on}(k) &= \frac{1 - S_{sw}(k)}{2\pi i} \\ &= \frac{1}{\pi}e^{-ikR}\,\frac{K\cos KR\sin kR - k\cos kR\sin KR}{K\cos KR - ik\sin Kr}. \end{aligned} \tag{6.16}$$

6.4 Half-off-shell T-matrix of the square well potential

The half-off-shell T-matrix is calculated by using Eq. (4.25). This equation contains the wave function with an outgoing spherical wave boundary condition which is given by Eq. (4.52). Since the potential is zero for all $r > R$, this boundary condition can be rewritten as

$$\langle \boldsymbol{x}|\psi^{(+)}\rangle = \frac{\sqrt{4\pi km}}{\hbar}\,\frac{1}{(2\pi)^{\frac{3}{2}}}\left(e^{i\boldsymbol{k}\cdot\boldsymbol{x}} + \frac{e^{ikr}}{r}f(\boldsymbol{k}',\boldsymbol{k})\right) \text{ for } r > R. \tag{6.17}$$

The plane wave can again be written as the sum of a spherically outgoing wave and a spherically incoming wave by using Eq. (4.43). For $r > R$ this results in

$$\langle \boldsymbol{x}|\psi^{(+)}\rangle = \frac{\sqrt{4\pi km}}{\hbar}\frac{1}{(2\pi)^{\frac{3}{2}}}\sum_l (2l+1)\frac{P_l(\cos\theta)}{2ik}\left(\big(1 + 2ikf_l(k)\big)\frac{e^{ikr}}{r} - \frac{e^{-i(kr-l\pi)}}{r}\right). \tag{6.18}$$

which can be simplified for low energy collisions. Inserting $l = 0$ for s-wave scattering and substituting Eq. (4.45) this equation can written as

$$\langle \boldsymbol{x}|\psi^{(+)}\rangle = \frac{\sqrt{4\pi km}}{\hbar}\frac{1}{(2\pi)^{\frac{3}{2}}}e^{i\delta_0(k)}\frac{\sin(kr+\delta_0(k))}{kr}. \tag{6.19}$$

A justification for neglecting partial waves with nonzero angular momenta can be found in Appendix A. Eq. (6.19) should be equal to $\frac{u(r)}{r}\frac{1}{\sqrt{4\pi}} = \frac{F\sin(kr+\delta_0)}{r}\frac{1}{\sqrt{4\pi}}$. So the outgoing spherical wave boundary condition gives

$$F = \frac{\sqrt{4\pi km}}{\hbar}\frac{1}{\sqrt{2}\pi}\frac{e^{i\delta_0(k)}}{k} = \frac{\sqrt{2\pi m}}{\hbar\pi}\frac{e^{i\delta_0(k)}}{\sqrt{k}}. \tag{6.20}$$

From Eq. (6.4) it follows that

$$A(k) = F\frac{\sin(kR+\delta_0)}{\sin KR} = \frac{\sqrt{2\pi m}}{\hbar\pi}\frac{e^{i\delta_0(k)}}{\sqrt{k}}\frac{\sin(kR+\delta_0)}{\sin KR}. \tag{6.21}$$

We have now obtained the full wave function with the outgoing spherical wave boundary condition. For $r < R$ it is given by

$$\langle \boldsymbol{x}|\psi^{(+)}\rangle = \frac{A(k)}{r\sqrt{4\pi}}\sin Kr \tag{6.22}$$

where $A(k)$ is given by Eq. (6.21). The plane-wave state in the integrand of Eq. (4.25) is given by

$$\langle \boldsymbol{k}'|\boldsymbol{x}'\rangle = \frac{\sqrt{4\pi k\prime m}}{\hbar}\frac{1}{(2\pi)^{\frac{3}{2}}}e^{-i\boldsymbol{k}\prime\cdot\boldsymbol{x}\prime}. \tag{6.23}$$

Here the energy normalization condition which is given by Eq. (4.50) has been used. For s-wave scattering we take only the s-wave part of the plane wave $\langle \boldsymbol{k}'|\boldsymbol{x}'\rangle$. The justification is given in Appendix A. So Eq. (4.25) can be approximated by using Eq. (4.34) and Eq. (4.35). The result is given by

$$\begin{aligned}\langle \boldsymbol{k}'|T|\boldsymbol{k}\rangle &= \int\int_0^\infty \langle \boldsymbol{k}'|E^*,0,0\rangle\langle E^*,0,0|\boldsymbol{x}'\rangle V(\boldsymbol{x}')\langle \boldsymbol{x}'|\psi^{(+)}\rangle dE^* d^3\boldsymbol{x}' \\ &= \frac{\sqrt{4\pi k'm}}{\hbar}\frac{1}{(2\pi)^{\frac{3}{2}}}\int \frac{\sin k'r'}{k'r'}V(\boldsymbol{x}')\langle \boldsymbol{x}'|\psi^{(+)}\rangle\, d^3\boldsymbol{x}' \\ &= \frac{\sqrt{4\pi k\prime m}}{\hbar}\frac{1}{(2\pi)^{\frac{3}{2}}}\int_0^\infty \frac{4\pi\sin k'r'}{k\prime r\prime}V(r')\langle \boldsymbol{x}'|\psi^{(+)}\rangle r'^2 dr'. \end{aligned}\tag{6.24}$$

In the last step the θ'- and φ'-integrals are evaluated. This is possible because the potential V is spherical symmetric and $\langle \boldsymbol{x}'|\psi^{(+)}\rangle$ is independent of θ' and φ' for s-wave scattering. Now the half-off-shell T-matrix of the finite square well potential (abbreviated as $T_{sw,half-off}$) is calculated for s-wave scattering by substituting Eq. (6.1) and Eq. (6.22) in Eq. (6.24). This gives

$$\begin{aligned}T_{sw,half-off}(k',k) &= \frac{\sqrt{4\pi k\prime m}}{\hbar}\frac{1}{(2\pi)^{\frac{3}{2}}}\int_0^R \frac{4\pi\sin k'r'}{k'r'}(-V_0)\left(\frac{A}{r\prime\sqrt{4\pi}}\sin Kr'\right)r'^2 dr' \\ &= -\frac{V_0 A(k)}{\sqrt{2}\pi k'}\frac{\sqrt{4\pi k\prime m}}{\hbar}\frac{1}{K^2-k'^2}(k'\cos k'R\sin KR - K\cos KR\sin k'R) \\ &= \frac{1}{\pi}\sqrt{\frac{k}{k'}}e^{-ikR}\frac{K^2-k^2}{K^2-k'^2}\,\frac{K\cos KR\sin k\prime R - k'\cos k\prime R\sin KR}{K\cos KR - ik\sin Kr}.\end{aligned}\tag{6.25}$$

The function $A(k)$ of Eq. (6.21) was used to simplify this equation. By setting $k' \to k$ in the half-off-shell T-matrix one obtains the on-shell T-matrix of the square well potential:

$$T_{sw,on}(k) = \frac{1}{\pi}e^{-ikR}\,\frac{K\cos KR\sin kR - k\cos kR\sin KR}{K\cos KR - ik\sin Kr}. \tag{6.26}$$

which equals the on-shell T-matrix of Eq. (6.16) as it should. Furthermore, the ratio of the half-off-shell T-matrix to the on-shell T-matrix is given by

$$\frac{T_{sw,half-off}(k',k)}{T_{sw,on}(k)} = \sqrt{\frac{k}{k'}}\frac{K^2-k^2}{K^2-k'^2}\frac{k'\cos k'R\sin KR - K\cos KR\sin k'R}{k\cos kR\sin KR - K\cos KR\sin kR}. \tag{6.27}$$

This energy normalized ratio is plotted in Fig. 6.3. This figure shows that the T-matrix oscillates and simultaneously decays to smaller and smaller values as you go off shell although initially it increases. The decay is characteristic of the finite range interaction, whereas the large number of oscillations is a characteristic of the sharp corners of the square well (Landau, 1996). When the normalization condition of Eq. (4.32) is used, Eq. (6.27) would be written as

$$\frac{T_{sw,half-off}(k',k)}{T_{sw,on}(k)} = \frac{k}{k'}\frac{K^2-k^2}{K^2-k'^2}\frac{k'\cos k'R\sin KR - K\cos KR\sin k'R}{k\cos kR\sin KR - K\cos KR\sin kR}. \tag{6.28}$$

This momentum normalized ratio is plotted in Fig. 6.4.[1] This figure shows that this ratio has no initial increase in contrast to the energy normalized ratio.

[1] This momentum normalized ratio $T_{sw,half-off}/T_{sw,on}$ for s-wave scattering differs slightly from the formula given on page 121 in the book *Quantum Mechanics II. A Second Course in Quantum Theory* written by Landau. The ratio given by Landau is inconsistent with the plot of this ratio which is also given in the book. Furthermore, the plot given in his book on page 120 cannot be correct since in his plot the ratio $T_{sw,half-off}/T_{sw,on}$ equals -1 for $k' = k$. Moreover, it looks like Landau has

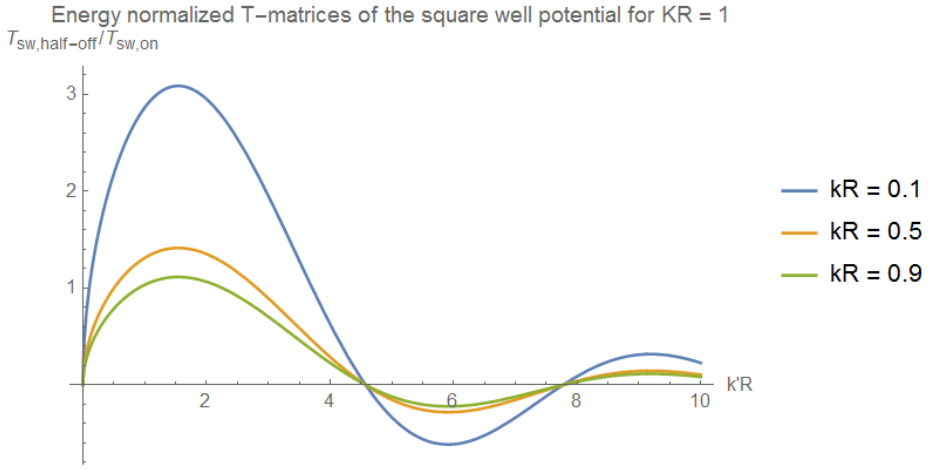

Fig. 6.3. Plot of the energy normalized ratio $T_{sw,half-off}/T_{sw,on}$ versus k'R for s-wave scattering by the square well potential with $KR = 1$. The value of kR is varied. It takes the values 0.1, 0.5 and 0.9.

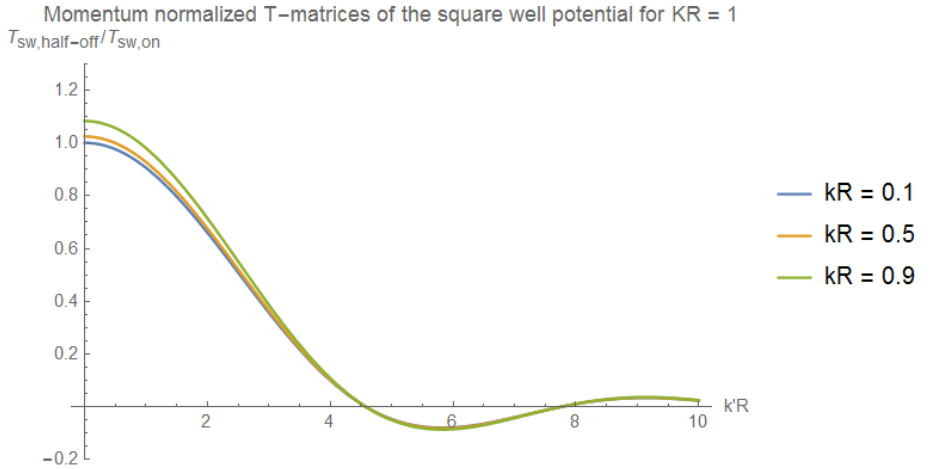

Fig. 6.4. Plot of the momentum normalized ratio $T_{sw,half-off}/T_{sw,on}$ versus k'R for s-wave scattering by the square well potential with $KR = 1$. The value of kR is varied. It takes the values 0.1, 0.5 and 0.9.

6.5 Off-shell wave function of the square well potential

The off-shell wave function of the square well for s-wave scattering is obtained by solving the off-shell Schrödinger equation (Eq. (4.30)) and applying the correct boundary conditions. We substitute Eq. (6.1) in Eq. (4.30) and solve this equation. The off-shell wave function is given by

$$u(r) = \begin{cases} A\,e^{-\frac{ir\sqrt{2m(V_0+z)}}{\hbar}} + B\,e^{\frac{ir\sqrt{2m(V_0+z)}}{\hbar}} + \frac{1}{(2\pi)^{\frac{3}{2}}}\frac{\sqrt{4\pi km}}{\hbar}\frac{2m(z-\frac{k^2\hbar^2}{2m})\sin kr}{k(2m(V_0+z)-k^2\hbar^2)} \;\; for\; r \le R \\ Ce^{\frac{ir\sqrt{2mz}}{\hbar}} + De^{-\frac{ir\sqrt{2mz}}{\hbar}} + \frac{1}{(2\pi)^{\frac{3}{2}}}\frac{\sqrt{4\pi km}}{\hbar k}\sin kr \;\; for\; r > R \end{cases} . \qquad (6.29)$$

Using the boundary condition which states that the wave function $\psi_{\boldsymbol{k}}(\boldsymbol{x},z) = u(r)/r$ is finite at $r = 0$ gives $A = -B$. Two other boundary conditions are the continuity of $u(r)$ and its derivative at $r = R$. Since we are interested in the off-shell wave function with an outgoing spherical wave boundary condition, we set $D = 0$ because this term represents an incoming spherical wave. We have now

---

plotted the energy normalized ratio $T_{sw,half-off}/T_{sw,on}$ although he calculated the momentum normalized ratio $T_{sw,half-off}/T_{sw,on}$.

obtained the fully off-shell wave function with the outgoing spherical wave boundary condition. The coefficients are given by

$$B = P\left(ik\hbar\cos kR + \sqrt{2mz}\sin kR\right) \tag{6.30}$$

and

$$C = 2Pe^{-\frac{iR\sqrt{2m(V_0+z)}}{\hbar}}\left(k\hbar\sin\left(\frac{\sqrt{2mz}}{\hbar}R\right)\cos kR - \sqrt{2m(V_0+z)}\cos\left(\frac{\sqrt{2mz}}{\hbar}R\right)\sin kR\right) \tag{6.31}$$

where P is given by

$$P = \frac{2mV_0}{\sqrt{k}\pi\hbar\,(2m(V_0+z)-k^2\hbar^2)}\left(\sqrt{V_0+z}\cos\frac{R\sqrt{2m(V_0+z)}}{\hbar} - i\sqrt{z}\sin\frac{R\sqrt{2m(V_0+z)}}{\hbar}\right)^{-1}. \tag{6.32}$$

It can be shown that the off-shell wave function reduces to the on-shell wave function of Eq. (6.19) and Eq. (6.22) in the limit $z \to \hbar^2k^2/2m$. The off-shell wave function contains only part of the information about the fully off-shell two-body T-matrix because it depends on only one momentum variable (the initial momentum) and not on the final momentum (Cheng et al., 1990).

6.6 Off-shell T-matrix of the square well potential

The fully two-body off-shell T-matrix of the square well potential is calculated by evaluating the integral of Eq. (6.24). However, the off-shell wave function for s-wave scattering should be used instead of the on-shell wave function. Substituting Eq. (6.1) and Eq. (6.29) in Eq. (6.24) gives

$$T_{sw,off}(k',k,q) = \frac{1}{\pi}\frac{1}{\sqrt{kk'}}\frac{K_E^2-q^2}{K_E^2-k^2}\cdot \left(g(K_E,k')(K_E^2-q^2)\frac{ik\cos kR+q\sin kR}{iK_E\cos K_ER+q\sin K_ER} + g(k,k')\,(q^2-k^2)\right). \tag{6.33}$$

In the derivation of this equation the complex energy has been taken to be real and it is given by $z = \hbar^2q^2/2m$ in which q can be either real or purely imaginary. The wave number K_E is a measure for the potential depth. The depth of the potential is given by $V_0 = \hbar^2(K_E^2-q^2)/2m$. Note that the depth of the potential is also given by $V_0 = \hbar^2(K^2-k^2)/2m$ as defined above. The function $g(k,k')$ is given by

$$g(k,k') = \frac{1}{k^2-k'^2}(k\cos kR\sin k'R - k'\cos k'R\sin kR). \tag{6.34}$$

It is possible to express the off-shell T-matrix in terms of the half-off-shell T-matrix. The result is

$$T_{sw,off}(k',k,q) = \frac{1}{\sqrt{kq}}\frac{K_E^2-q^2}{K_E^2-k^2}e^{iqR}\,(k\cos kR - iq\sin kR)\cdot (T_{sw,half-off}(k',q,V_0) - T_{sw,half-off}(k',q,V^*)). \tag{6.35}$$

Here $T_{sw,half-off}(k',q,V)$ is just the half-off-shell T-matrix for a square well potential with depth V and initial momentum q and is given by Eq. (6.25). The potential depth V^* is given by

$$V^* = \frac{\hbar^2}{2m}(k^2-q^2). \tag{6.36}$$

Note that V^* goes to zero when $q \to k$ and therefore $T_{sw,half-off}(k',q,V^*)$ goes to zero in this limit. It can be checked that the fully-off-shell T-matrix reduces to the half-off-shell T-matrix by setting $q \to k$ in Eq. (6.35). Also note that $T_{sw,off}(k',k,q)$ is real for negative energies, i.e. when q is imaginary. Furthermore, it can be shown that the off-shell T-matrix is symmetric. It satisfies

$$T_{sw,off}(k', k, q) = T_{sw,off}(k, k', q). \tag{6.37}$$

Fig. 6.5 en 6.6 show this symmetry of $T_{sw,off}(k', k, q)$. These figures also illustrate the strong influence of the momenta on the behavior of the off-shell T-matrix which decays as you go off shell. The oscillatory behavior is a characteristic of the sharp corners of square well. In Fig. 6.7 the dependence of the T-matrix on q is investigated. The momentum normalized T-matrix is plotted. It is obtained by multiplying Eq. (6.33) with $\frac{\hbar^2}{4\pi m\sqrt{k'k}}$. Note that the momentum normalized T-matrix does not start at the origin. The absolute value of $T_{sw,off}(k', k, q)$ increases when q goes to zero. As $q \to 0$ the absolute value of the T-matrix goes to infinity at $k' = k = 0$.

Finally, Fig. 6.8 shows that the maximum of $T_{sw,off}(k', k, q)$ shifts when the depth of the square well potential increases. Here the wavenumber K_0 is defined by $K_0 = \sqrt{\frac{2mV_0}{\hbar^2}}$. This maximum peak occurs at $k'R = K_0R$. Additional figures of the off-shell T-matrix can be found in Appendix B. Fig. B.1 shows that when the resonant condition is not fulfilled, the maximum peak still occurs $k'R = 0$ although a smaller peak at $k'R = K_0R$ is also present. For higher values of $k'R$ the T-matrix oscillates and simultaneously decays to smaller and smaller values.

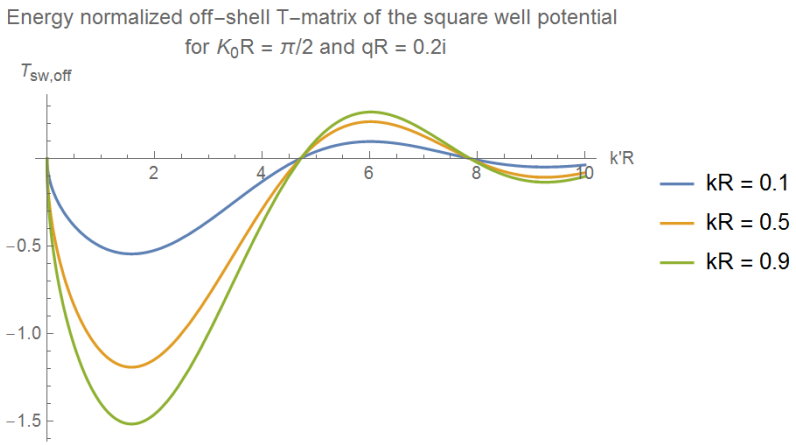

Fig. 6.5. Plot of the energy normalized $T_{sw,off}$ versus k'R for s-wave scattering by the square well potential with $K_0R = \pi/2$ and $qR = 0.2i$. The value of kR is varied. It takes the values 0.1, 0.5 and 0.9.

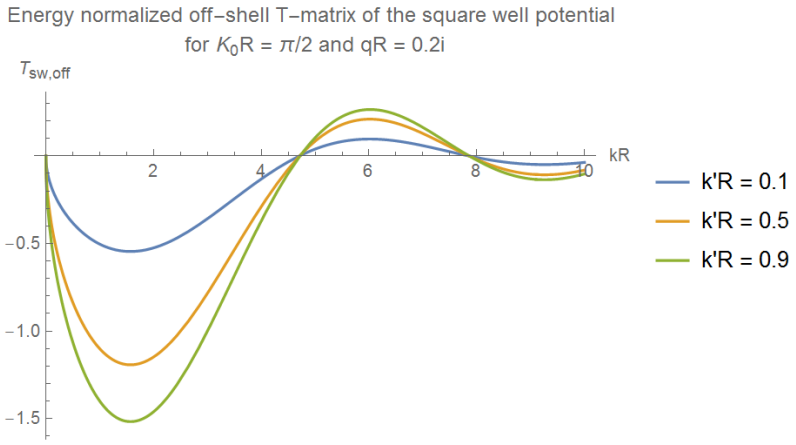

Fig. 6.6. Plot of the energy normalized $T_{sw,off}$ versus kR for s-wave scattering by the square well potential with $K_0R = \pi/2$ and $qR = 0.2i$. The value of k'R is varied. It takes the values 0.1, 0.5 and 0.9.

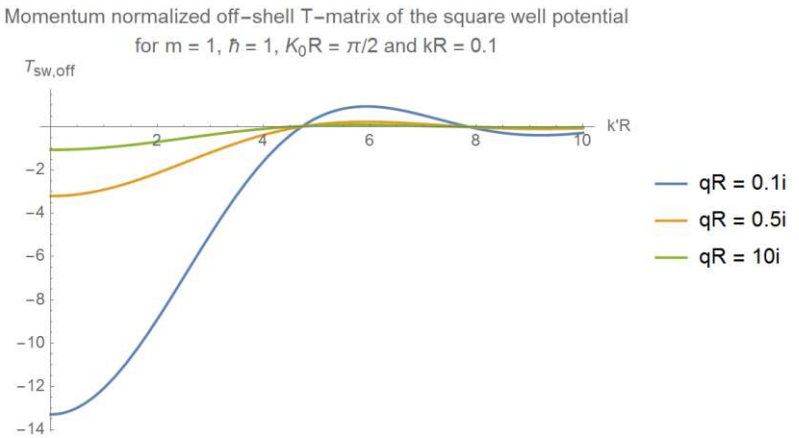

Fig. 6.7. Plot of the momentum normalized $T_{sw,off}$ *versus* $k'R$ *for s-wave scattering by the square well potential with* $m = 1$, $\hbar = 1$, $K_0R = \pi/2$ *and* $kR = 0.1$. *The value of* qR *is varied. It takes the values 0.1i, 0.5i and 10i.*

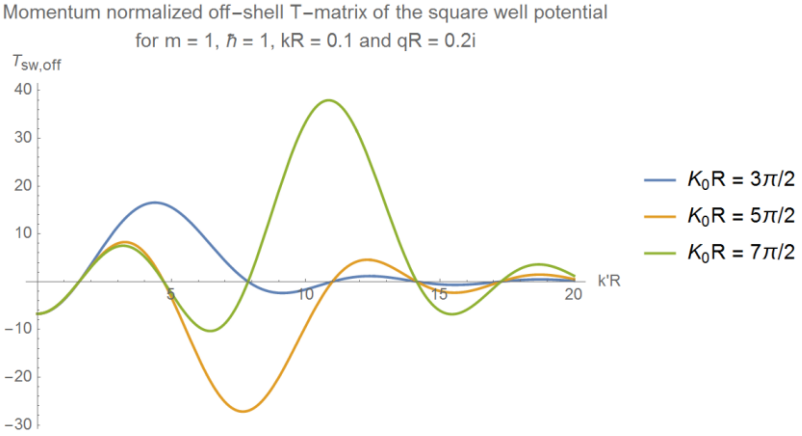

Fig. 6.8. Plot of the momentum normalized $T_{sw,off}$ *versus* $k'R$ *for s-wave scattering by the square well potential with* $m = 1$, $\hbar = 1$, $qR = 0.2i$ *and* $kR = 0.1$. *The value of* K_0R *is varied. It takes the values* $3\pi/2$, $5\pi/2$ *and* $7\pi/2$.

The off-shell T-matrix of Eq. (6.33) has been checked with the off-shell T-matrix calculated by H. Cheng, E. Vilallonga and H. Rabitz (Cheng et al., 1990). In their article the off-shell T-matrix elements for scattering from the spherical hard-core plus square-well potential is calculated. This potential is given by

$$V = \begin{cases} \infty & for\ r \le a \\ -V_0 & for\ a < r < b. \\ 0 & for\ r \ge b \end{cases} \tag{6.38}$$

In the limit $a \to 0$ this potential reduces to the square well potential. We have confirmed that the T-matrix of (Cheng et al., 1990) for s-wave scattering reduces to Eq. (6.33) in this limit.[2] Since the fully off-shell T-matrix calculated by H. Cheng, E. Vilallonga and H. Rabitz (Cheng et al., 1990) contains partial-wave elements, their off-shell T-matrix can be used to check that it is justified to consider only the s-wave scattering contribution to the off-shell T-matrix. This justification is given in Appendix A.

[2] In the article (Cheng et al., 1990) the momentum normalization convention has been used, i.e. $\langle \boldsymbol{p}|\boldsymbol{p}'\rangle = \delta^{(3)}(\boldsymbol{p}-\boldsymbol{p}')$. The momentum normalized T-matrix should be multiplied with $4\pi m\sqrt{p\,p'}$ to obtain the energy normalized T-matrix. Here the momentum $p = \hbar k$ and $p' = \hbar k'$.

7. Model setup

The potential resonance of the square well potential, which has been studied in the previous section, is used to simulate a Feshbach resonance and calculate the Efimov spectrum. Furthermore, the universality of the three-body parameter $a_0^{(-)}$ is investigated. The results will be given in the next chapter. In this chapter the model is explained. It is implemented in Mathematica. This numerical part of the report is the extension of my bachelor thesis which encompasses 5 ECTS.

The model is based on T.J. Rademaker's model (Rademaker, 2014) who used a simplified off-shell two-body T-matrix for a Feshbach resonance. His T-matrix is factorized into three parts: one factor which depends only on the energy wavenumber q and two Gaussion cutoff functions of which one depends on the initial momentum k and the other depends on the final momentum k'. This T-matrix is compared with the off-shell T-matrix of the square well potential in Appendix C. From this comparison we expect quite similar results for $K_0R = \pi/2$. However, Rademaker's T-matrix is absolutely not similar to the off-shell T-matrix of the square well for $K_0R = n\pi/2$ with n = 3, 5, 7 etc. So the effect of deeper lying two-body bound states on the Efimov spectrum is an interesting topic. Although Rademaker's model does not include real off-shell two-body interactions, it has given us insight in the effects of the effective range and Gaussian cutoff function on the universality of the three-body parameter. The square well model which will be used in this report also does not describe real interactions between atoms. However, it should give us more insight into the effects of both off-shell interactions and deeper lying two-body bound states on the binding energies of the Efimov trimers. Furthermore, the off-shell T-matrix has been calculated exactly, so no artificial cutoff function is needed to retrieve a three-body parameter.

7.1 The angular dependence of the STM-equation

The STM-equation given by Eq. (5.3) can be used to find the binding energies of the Efimov trimers. For s-wave scattering $T_3(k)$ and $T_2(k', k, \hbar^2q^2/m)$ do not depend on the scattering angles. However, the arguments $\left|\boldsymbol{k} - \frac{\boldsymbol{p}}{2}\right|$ and $\left|\boldsymbol{p} - \frac{\boldsymbol{k}}{2}\right|$ depend on the angle between $\boldsymbol{p}$ and $\boldsymbol{k}$. Just like (Levinsen, 2013) we will simplify the equation by the following replacements: $\left|\boldsymbol{k} - \frac{\boldsymbol{p}}{2}\right| \to k$ and $\left|\boldsymbol{p} - \frac{\boldsymbol{k}}{2}\right| \to p$. A justification is given in Appendix D. It seems that this approximation is only valid for a square well potential with $K_0R \approx \pi/2$. With this simplification angular averaging of Eq. (5.3) leads to

$$T_3(k) = \frac{m}{2\pi^2 k}\int p\, T_2\left(p, k, E - \frac{3k^2}{4m}\right) \ln\left(\frac{E - k^2/m - p^2/m + kp/m}{E - k^2/m - p^2/m - kp/m}\right) T_3(p)dp. \tag{7.1}$$

The derivation of this equation is also given in Appendix D.

7.2 STM-equation for a square well potential

The two-body off-shell T-matrix of the square well potential was derived in section 6.6. Now we will substitute this T-matrix in the STM-equation and calculate the trimer energy $E = -\frac{3{q_3}^2}{4m}$ as a function of the inverse two-body scattering length $1/a$, where

$$a = R\left(1 - \frac{\tan K_0R}{K_0R}\right). \tag{7.2}$$

So the potential resonance of the square well potential is used to simulate a Feshbach resonance. Substitution of the trimer energy $E = -\frac{3{q_3}^2}{4m}$ in Eq. (7.1) gives

$$T_3(k) = \frac{m}{2\pi^2 k}\int p\, T_2\left(p, k, -\frac{3}{4m}({q_3}^2 + k^2)\right) \ln\left(\frac{\frac{3}{4}{q_3}^2 + k^2 + p^2 - kp}{\frac{3}{4}{q_3}^2 + k^2 + p^2 + kp}\right) T_3(p)dp. \tag{7.3}$$

So in the T-matrix $T_2(k', k, \hbar^2 q^2/m)$ for the square well potential q should be replaced by $i\frac{\sqrt{3}}{2}\,({q_3}^2 + k^2)$.

7.3 Efimov trimer states

The STM-equation is a homogenous Fredholm equation of the second kind. It is numerically solvable. For more information about numerically solving Fredholm integral equations the book Numerical Recipes by Press, Teukolsky, Vetterling and Flannery (Press, 2007) can be consulted.

We solve Eq. (7.3) by considering the eigenvalues of the kernel K. In Eq. (7.3) the kernel is given by

$$K(p,k) = \frac{m}{2\pi^2 k}\, p\, T_2\left(p, k, -\frac{3}{4m}({q_3}^2 + k^2)\right) \ln\left(\frac{\frac{3}{4}{q_3}^2 + k^2 + p^2 - kp/m}{\frac{3}{4}{q_3}^2 + k^2 + p^2 + kp/m}\right). \tag{7.4}$$

An appropriate grid for the momenta k and p is chosen by the method Gaussian Quadrature Weights. This method is suitable for a smooth, nonsingular integrand, which is the case in Eq. (7.3), because then Gaussian quadratures converges exponentially fast as the number of grid points increases. It is the most efficient quadrature rule for nonsingular functions (Press, 2007). The basic idea behind Gaussian quadrature is to approximate the value of an integral as a linear combination of values of the integrand evaluated at specific points x_i and weighted by a specific number w_i (Press, 2007), i.e.

$$\int_a^b f(x)\, dx = \sum_{i=1}^{n} w_i\, f(x_i). \tag{7.5}$$

Next, the homogenous Fredholm equation (Eq. (7.3)) can be written in matrix form as follows:

$$T_i = \sum_{j=1}^{n_k} K_{ij} T_j. \tag{7.6}$$

Here n_k is the number of grid points for the momenta k and p and it fixes the size of the kernel. The smaller the number of grid points, the faster the computation will be. However, if more grid points are used, the result will be more accurate. The kernel K_{ij} is just $K(p,k)dp$ where p is constant in each column and varies in the rows, whereas k is constant in each row and varies in the columns.

Eq. (7.6) is an eigenvalue equation in which all the eigenvalues of the kernel are equal to one. So the Efimov trimers should obey

$$\det\big(I - [K_{ij}]\big) = 0. \tag{7.7}$$

Here I is the $n_k \times n_k$ identity matrix. The matrix $[K_{ij}]$ depends on the energy momentum q_3 and the depth of the potential K_0. The range of the potential will be fixed in this report. The Efimov trimers only obey Eq. (7.7) for specific values of q_3 and K_0 when the potential range R is fixed. The goal will be to obtain these values and to plot the trimer energy $E = -\frac{3{q_3}^2}{4m}$ as a function of the inverse two-body scattering length $1/a(K_0, R)$.

Note that the square well potential contains infinitely many values for K_0R for which the scattering length diverges. In this report only one grid for K_0 will be chosen. The Efimov bound states are found around $K_0R = \frac{\pi}{2}$, which means that no two-body bound state exists for K_0R below $\pi/2$ and only one two-body bound state exists for K_0R slightly greater than $\pi/2$. The Efimov spectrum is not calculated at the resonant condition $K_0R = n\pi/2$ with n = 3, 5, 7, etc. because Levinsen's approximation is not valid in this case.

Furthermore, the model contains an energy grid q_3. For each value of q_3 the determinant

$\det\left(I - [K_{ij}]\right)$ is calculated for all K_0 of the K_0 grid, which is related to negative scattering lengths, until the first zero is found. Then the next value for q_3 is substituted in the determinant and the determinant is calculated for K_0 values close to the one which was found before. This procedure is repeated until q_3 exceeds the three-body parameter $2\kappa_*/\sqrt{3}$ and no zeroes are found for this Efimov trimer state for negative scattering lengths. Then a new K_0 grid is defined which is related to positive scattering lengths and the procedure described above is repeated for the remaining q_3 values of the energy grid.

For a particular trimer state, the result will be a table which contains the trimer energy $E = -\frac{3{q_3}^2}{4m}$ and the corresponding K_0 values from which the scattering length can be calculated. Then the trimer energy is plotted as a function of the inverse scattering length. In order to plot several trimer states in one diagram the Efimov spectrum will be rescaled in the same way as T.J. Rademaker has done (Rademaker, 2014). This means that $\text{sign}(E)\left|\left(a_0^{(-)}\right)^2 E\right|^{1/8}$ is plotted versus $\text{sign}(a)\left|a_0^{(-)}/a\right|^{1/4}$.

7.4 Dissociation threshold

Not only the trimer states will be plotted, but also the dissociation threshold, which is the weakly bound dimer state. The dissociation threshold for the three-body bound state at rest is given by Eq. (6.14). Substituting Eq. (6.12) in the two-body bound state energy gives

$$E = -\frac{\hbar^2\kappa^2}{m} = -\frac{\hbar^2}{m}K^2(\cot KR)^2 \tag{7.8}$$

Note that m in Eq. (6.14) is the reduced mass of the two-particle system as explained in section 4.1. and it equals $\frac{1}{2}m$. The binding energy of the dimer state is $E = -\frac{\hbar^2{q_2}^2}{m}$. So from Eq. (7.8) it follows that

$$q^2 = (K_0^2 + q^2)\cot\left(\sqrt{K_0^2 + q^2}R\right) \tag{7.9}$$

where now $q = iq_2$. This equation can also be written as

$${q_2}^2 = (K_0^2 - {q_2}^2)\cot\left(\sqrt{K_0^2 - {q_2}^2}R\right). \tag{7.10}$$

Again K_0 is related to the scattering length by Eq. (7.2). So this transcendental equation should be solved numerically for K_0 for each value of q_2. Next, the s-wave scattering length is calculated and the dimer binding energy can be plotted.

8. Results and discussion

In this section the results of the model which is described in the previous chapter are shown. The Efimov spectrum is calculated and the universality of the three-body parameter $a_0^{(-)}$ is investigated. In this chapter the width of the square well potential is fixed. It is chosen that $R = 50$. All quantities with units of length are chosen to be dimensionless. Uncertainties of the results are not given because there is no simple way to estimate the error in the results obtained by a method based on Gaussian quadrature (Press, 2007). Furthermore, the approximations used to simplify the STM-equation will also increase the uncertainty of the results in a complex way. However, the chosen grids for K_0, k and q give an upper limit for the number of significant figures.

The first five Efimov bound states with a square well potential as two-body interaction are shown in Fig. 8.1. At $1/a = 0$ the resonance condition $K_0 R = \pi/2$ is fulfilled. More details about this plot can be found in Table 8.1. Some three-body parameters are indicated in the figure. Furthermore, the parameters $a^{(+)}$ are also indicated. These parameters represent the value of the scattering length for which a particular trimer state has converged to the two-body bound state energy.

An important characteristic of the calculated Efimov spectrum is the absence of the parameter $a_0^{(+)}$. The energy of the lowest-energy three-body bound state does not converge to the two-body bound state energy. The effect of this phenomenon is unclear. More research should be done to understand this characteristic of the Efimov spectrum. The absence of the parameter $a_0^{(+)}$ could be caused by the numerical method (for example the simplifications in the STM-equation). It is also possible that the lowest-energy Efimov state converges to an ordinary three-body bound state of the interaction potential which is lying close to the collision threshold.

It is very interesting whether this phenomenon is also present in the Efimov spectrum with a square well potential as two-body interactions with higher resonance conditions ($K_0 R = n\pi/2$ with n = 3, 5, 7, etc.). It is likely that the Efimov spectrum will be different because Fig. 6.1 shows that the width of the resonance decreases when the product $K_0 R$ increases. As will be discussed below, it is likely that the three-body parameter $a_0^{(-)}$ increases for deeper square well potentials. If this is the case, the lowest energy three-body bound state shifts upward in the Efimov spectrum. As a result, it could be possible that in this case the parameter $a_0^{(+)}$ is not absent, so that also the first Efimov state converges to the two-body bound state energy.

Fig. 8.1 shows that the energy of the three-body bound states (except for the lowest-energy Efimov trimer state) exceeds the two-body bound state energy which cannot be correct. Furthermore, these higher-energy trimer states are not smooth for positive values of the inverse scattering length. This indicates that the numerical solving method is not accurate enough. This is probably the result of the chosen grids for K_0 and k. Although the K_0 grid contains 2005 values in the positive scattering length region, more values will certainly increase the accuracy. This is also true for the k grid. However, larger grids for K_0 and k will result in longer computation times, but the Efimov spectrum will be smoother.

Table 8.1 shows several parameters of the Efimov bound states which were plotted in Fig. 8.1. No more than two significant figures can be given due to the chosen grid for K_0. It is expected that a larger K_0 grid can give a more accurate result for the three-body parameters. Furthermore, the q grid which is used to obtain the results of Table 8.1, cannot lead to κ^* values with more than one significant figure. The energy grid should contain more momenta q to retrieve κ^* values with higher accuracy.

Since the width of the square well was chosen to be $R = 50$, the first Efimov bound state is expected to have a three-body parameter at $a_0^{(-)} = -9.8\, R_{vdW} \approx -9.8\, R = -5 \cdot 10^2$. However, Table 8.1

shows that $a_0^{(-)} = -1.5 \cdot 10^2 = -3\,R$. The fact that the universal value of the three-body parameter has not been retrieved for the resonance condition $K_0 R = \pi/2$ means that this square well potential is not representative for the two-body interaction potential between ultracold atoms whose long-range behavior is governed by the van der Waals interaction. Since the three-body parameter has a universal value for deep potentials decaying faster than $1/r^6$ (Horinouchi & Ueda, 2015), it will only be retrieved if the dimensions of the square well are chosen such that this criterion is fulfilled. So the parameter $K_0 R$ is probably too small to retrieve the universal value of the three-body parameter. So, the potential resonance at $K_0 R = n\pi/2$ in which n is an odd number greater one, has to be studied to retrieve the universal value of $a_0^{(-)}$.

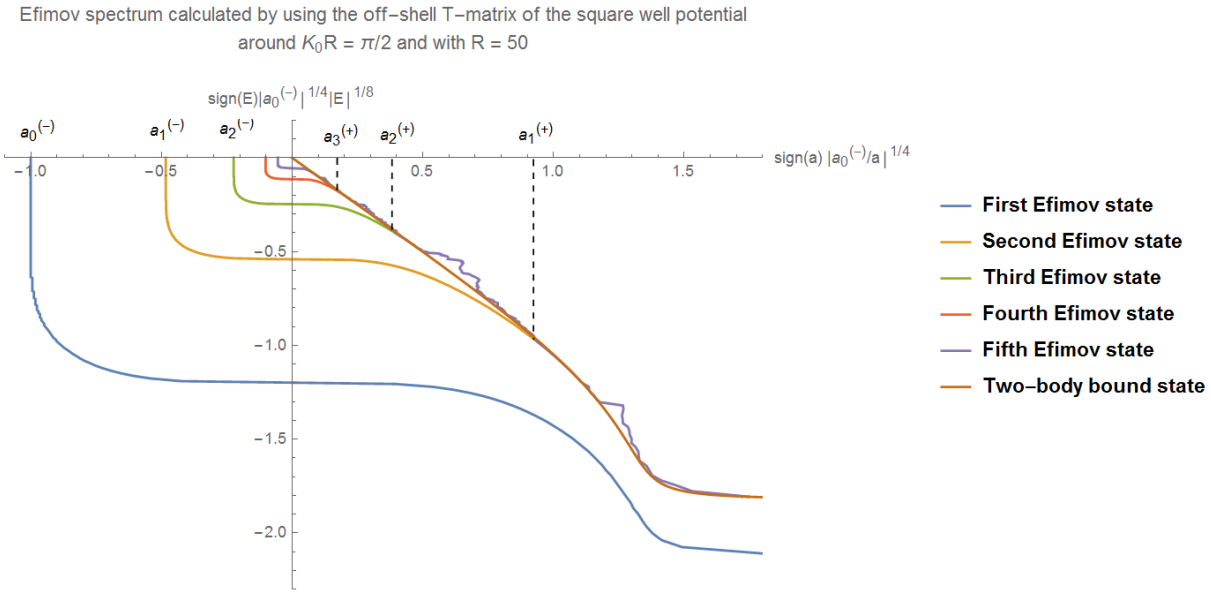

Fig. 8.1. First five Efimov bound states with a square well potential as two-body interaction. The width of the potential is $R = 50$. The depth of the potential is chosen such that $\frac{1}{a} = 0$ corresponds to $K_0 R = \pi/2$. The number of grid points is $n_k = 150$. The values of the three-body parameters is shown in Table 8.1. The brown curve is the two-body bound state energy which is calculated with Eq. (7.10). The calculation takes approximately 85 minutes per trimer state.

Table 8.1: Several parameters of the Efimov bound states with a square well potential as two-body interaction. The width of the potential is $R = 50$. The depth of the potential is chosen such that $\frac{1}{a} = 0$ corresponds to $K_0 R = \pi/2$. The number of grid points is $n_k = 150$. For negative scattering lengths, the K_0 grid contains 600 values which results in 600 values for $1/a$ between $-1.3 \cdot 10^{-9}$ and -0.37. For positive scattering lengths, the K_0 grid contains 2005 values which results in 2005 values for $1/a$ between $7.7 \cdot 10^{-10}$ and 2.0. The three-body parameter κ^* has been defined in Eq. (2.2).

$a^{(-)}$	$a^{(+)}$	κ^*	*Scaling factors for* $a^{(-)}$	*Scaling factors for* κ^*
$a_0^{(-)} = -1.5 \cdot 10^2$	-	$\kappa_0^* = 1 \cdot 10^{-2}$	$a_1^{(-)}/a_0^{(-)} = 18$	$\kappa_0^*/\kappa_1^* = 2 \cdot 10^1$
$a_1^{(-)} = -2.7 \cdot 10^3$	$a_1^{(+)} = 2.0 \cdot 10^2$	$\kappa_1^* = 6 \cdot 10^{-4}$	$a_2^{(-)}/a_1^{(-)} = 22$	$\kappa_1^*/\kappa_2^* = 2 \cdot 10^1$
$a_2^{(-)} = -5.9 \cdot 10^4$	$a_2^{(+)} = 6.0 \cdot 10^3$	$\kappa_2^* = 3 \cdot 10^{-5}$	$a_3^{(-)}/a_2^{(-)} = 24$	$\kappa_2^*/\kappa_3^* = 2 \cdot 10^1$
$a_3^{(-)} = -1.4 \cdot 10^6$	$a_3^{(+)} = 1.4 \cdot 10^5$	$\kappa_3^* = 1 \cdot 10^{-6}$	$a_4^{(-)}/a_3^{(-)} = 12$	$\kappa_3^*/\kappa_4^* = 2 \cdot 10^1$
$a_4^{(-)} = -1.7 \cdot 10^7$	$a_4^{(+)} = 4.6 \cdot 10^7$	$\kappa_4^* = 6 \cdot 10^{-8}$		

The accuracy of the scaling factors will increase if a larger K_0 grid is chosen. Table 8.2 shows the scaling factors for the case in which 1.6 times more grid points for K_0 were used. The corresponding plot of $\det(I - [K_{ij}])$ as a function of $\ln(1/|a|)$ is shown in Fig. 8.2. The determinant has five zeroes which correspond to the three-body parameters of the first five lowest-energy Efimov trimer states. The difference between Table 8.1 and Table 8.2 is that the third scaling factor $a_3^{(-)}/a_2^{(-)}$ is closer to the universal value 22.7 in Table 8.2. This is a logical result because more grid points for K_0 increases the accuracy.

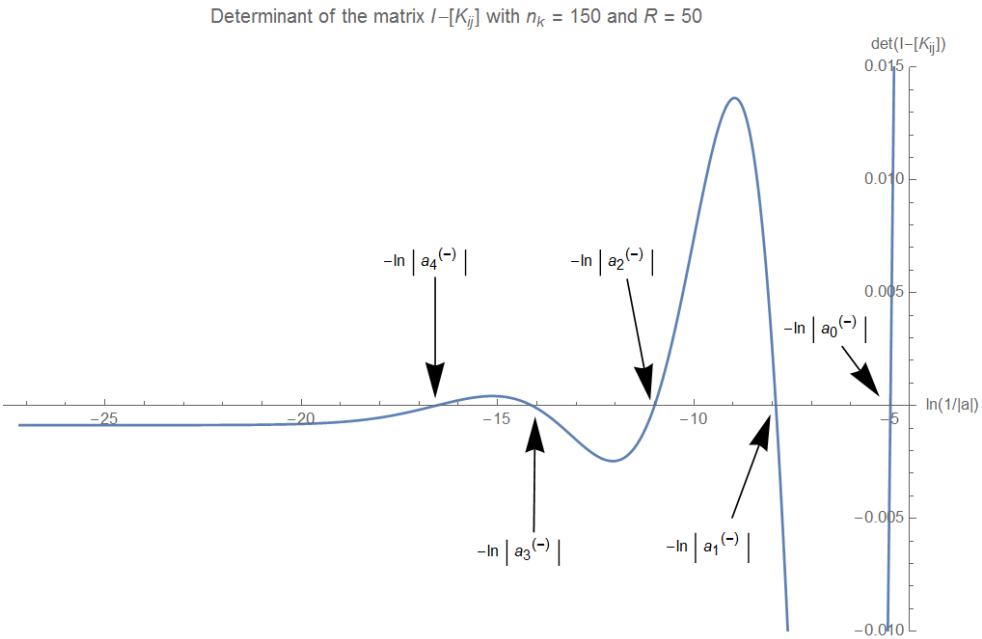

Fig. 8.2. Plot of $\det(I - [K_{ij}])$ *as a function of* $\ln(1/|a|)$ *at* $E = 0$ *for* $n_k = 150$. *Five zeroes which correspond to the three-body parameters of the first five lowest-energy Efimov trimer states are clearly visible. These zeroes of* $\ln(1/|a|)$ *are -16.6, -14.1, -11.0, -7.92 and -5.00. Since the universal scaling factor is* $e^{\pi/s_0} \approx e^{3.1}$, *the distance between the zeroes is expected to be 3.1 which is the case for* $a_2^{(-)}$ *and* $a_1^{(-)}$ *and for* $a_3^{(-)}$ *and* $a_2^{(-)}$. *Note that the three-body parameters corresponding to higher energy bound states (i.e.* $a_5^{(-)}$, $a_6^{(-)}$, *etc.) cannot be determined from this calculation because the matrix size is too small. More details are given in Table 8.2.*

Table 8.2: Several parameters of the Efimov bound states with a square well potential as two-body interaction. The width of the potential is $R = 50$. *The depth of the potential is chosen such that* $\frac{1}{a} = 0$ *corresponds to* $K_0 R = \pi/2$. *The number of grid points is* $n_k = 150$. *The* K_0 *grid contains 989 values which resulted in 989 values for* $1/a$ *between* $-1.6 \cdot 10^{-12}$ *and* -0.37. *The corresponding plot of* $\det(I - [K_{ij}])$ *as a function of* $\ln(1/|a|)$ *is shown in Fig. 8.2.*

Three-body parameter a^-	*Scaling factors*
$a_0^{(-)} = -1.5 \cdot 10^2$	$a_1^{(-)}/a_0^{(-)} = 18$
$a_1^{(-)} = -2.7 \cdot 10^3$	$a_2^{(-)}/a_1^{(-)} = 22$
$a_2^{(-)} = -6.0 \cdot 10^4$	$a_3^{(-)}/a_2^{(-)} = 23$
$a_3^{(-)} = -1.4 \cdot 10^6$	$a_4^{(-)}/a_3^{(-)} = 12$
$a_4^{(-)} = -1.6 \cdot 10^7$	

The results of Table 8.1 and 8.2 have been obtained with a small momentum grid for k. Table 8.3 shows the scaling factors for the case in which twice as many grid points are used ($n_k = 300$). The corresponding plot of $\det(I - [K_{ij}])$ as a function of $\ln(1/|a|)$ is shown in Fig. 8.3. Now the determinant has six zeroes which correspond to the three-body parameters of the first six lowest-energy Efimov trimer states. This shows that increasing the matrix size leads to the identification of more trimer states.

The calculation of Table 8.3 which involves only one energy value, namely $q = 0$, takes approximately 50 minutes. For comparison, a similar calculation for $n_k = 150$, which has leaded to the results shown in Table 8.2, takes approximately 20 minutes. Therefore, the Efimov spectrum, which includes at least 300 values for q, was only calculated for $n_k = 150$.

The first four three-body parameters in Table 8.2 and Table 8.3 are the same. However, the three-body parameter $a_4^{(-)}$ is different. As a result, the scaling factor $a_4^{(-)}/a_3^{(-)}$ in Table 8.3 is closer to the universal scaling factor than in Table 8.2 as it should be. After all, more grid points should give a more accurate result. It is not surprisingly that the scaling factor $a_5^{(-)}/a_4^{(-)}$ is far from the universal scaling factor. This is due to the fact that the highest energy Efimov trimer state which can be found by using this numerical solving method is often inaccurate. The determinant of Eq. (7.7) has no zeroes for scattering lengths $|a| > \left|a_5^{(-)}\right|$. If more grid points n_k were used, the scaling factor $a_5^{(-)}/a_4^{(-)}$ would also approach the universal scaling factor and higher energy Efimov trimer states would appear.

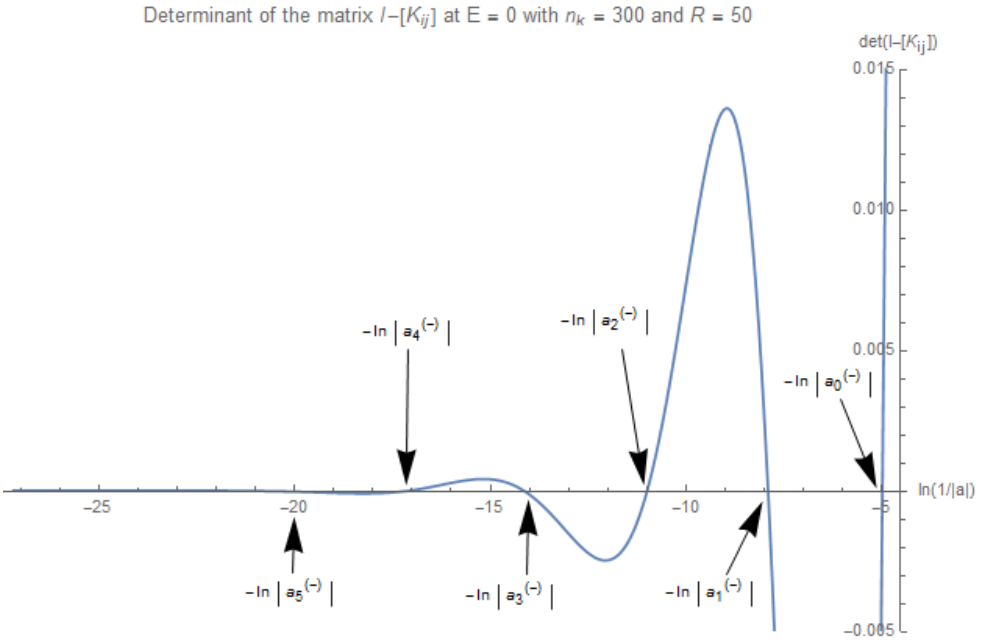

Fig. 8.3. Plot of $\det(I - [K_{ij}])$ *as a function of* $\ln(1/|a|)$ *at* $E = 0$ *for* $n_k = 300$. *Six zeroes which correspond to the three-body parameters of the first six lowest-energy Efimov trimer states are clearly visible. These zeroes of* $\ln(1/|a|)$ *are -20.4, -17.2, -14.1, -11.0, -7.92 and -5.00. Since the universal scaling factor is* $e^{\pi/s_0} \approx e^{3.1}$, *the distance between the zeroes is expected to be 3.1 which is the case for* $a_2^{(-)}$ *and* $a_1^{(-)}$, *for* $a_3^{(-)}$ *and* $a_2^{(-)}$ *and for* $a_4^{(-)}$ *and* $a_3^{(-)}$. *Note that the three-body parameters corresponding to higher energy bound states (i.e.* $a_6^{(-)}$, $a_7^{(-)}$, *etc.) cannot be determined from this calculation because the matrix size is too small. More details are given in Table 8.3.*

Table 8.3: Several parameters of the Efimov bound states with a square well potential as two-body interaction. The width of the potential is $R = 50$. The depth of the potential is chosen such that $\frac{1}{a} = 0$ corresponds to $K_0 R = \pi/2$. The number of grid points is $n_k = 300$. The K_0 grid contains 989 values which resulted in 989 values for $1/a$ between $-1.6 \cdot 10^{-12}$ and -0.37. The corresponding plot of $det(I - [K_{ij}])$ as a function of $ln(1/|a|)$ is shown in Fig. 8.3.

Three-body parameter $a^{(-)}$	*Scaling factors*
$a_0^{(-)} = -1.5 \cdot 10^2$	$a_1^{(-)}/a_0^{(-)} = 18$
$a_1^{(-)} = -2.7 \cdot 10^3$	$a_2^{(-)}/a_1^{(-)} = 22$
$a_2^{(-)} = -6.0 \cdot 10^4$	$a_3^{(-)}/a_2^{(-)} = 23$
$a_3^{(-)} = -1.4 \cdot 10^6$	$a_4^{(-)}/a_3^{(-)} = 22$
$a_4^{(-)} = -3.0 \cdot 10^7$	$a_5^{(-)}/a_4^{(-)} = 25$
$a_5^{(-)} = -7.5 \cdot 10^8$	

The lowest-energy trimer states are the most interesting ones because non-universality of the scaling factor will occur if the scattering length approaches the effective range. The effective range can be calculated with Eq. (6.9). For $a = a_0^{(-)}$, the effective range equals $R_e = 70$. Since the absolute value of the scattering length is greater than the effective range for all Efimov trimer states in the Borromean region, finite range effects will be small. Table 8.2 and Table 8.3 show that the first scaling factor is $a_1^{(-)}/a_0^{(-)} = 18$ which deviates from the universal scaling factor 22.7. This deviation could be the result of finite range effects. However, it is also possible that this scaling factor is in fact universal, but that the uncertainty in the result is too high, so that $a_1^{(-)}/a_0^{(-)} = 18$ is not an accurate result. If this is the case, the inaccuracy would not be caused by the chosen grid for K_0 because this grid has been chosen large enough to express the scaling factor in two significant figures. In this case, the inaccuracy would be caused by the approximations used in the STM-equation or the chosen grid for k. However, it is difficult to estimate the uncertainty caused by the chosen grid for k. Since the scaling factors calculated for both $n_k = 150$ and $n_k = 300$ are the same, namely $a_1^{(-)}/a_0^{(-)} = 18$, it seems reasonable to assume that the chosen grid for k is accurate enough and that the first two figures of the calculated scaling factor $a_1^{(-)}/a_0^{(-)}$ are significant. This means that the deviation of the first scaling factor from the universal scaling factor 22.7 is probably the result of finite range effects although it could also be caused by the approximations used in the STM-equation.

It has been shown that if the size of the matrices is larger, more zeroes are found at high scattering lengths. The scaling factor of the three-body parameters $a^{(-)}$ of the two highest energy Efimov trimers often differs from the universal scaling factor 22.7. This is an artefact of the solving method. If the matrix size would be further increased, the scaling between these two zeroes of the determinant will approach 22.7 and an additional zero is found at a higher scattering length. Again, the scaling factor between the three-body parameters of the two highest energy Efimov trimers will not be exactly 22.7.

Increasing the matrix size leads to a significantly increased computation time of the model. Therefore, the matrix size should be large enough to identify some Efimov trimers with a three-body parameter which is much larger than the range of the potential, so that the universal scaling factor is recovered. However, the matrix size should not be too large because the time to calculate the Efimov spectrum increases significantly.

If more accurate grids for K_0 and k are chosen, the three-body parameters can be expressed in three significant figures. However, this will increase the computation time significantly. This is an

disadvantage of the numerical method used. Probably, a faster computation method is needed to calculate the Efimov spectrum with high accuracy in short computation times. Note that the off-shell two-body T-matrix of Eq. (6.33) is proportional to K_0^2. So one possible method is to write the STM-equation with the square well potential as two-body interaction as

$$\frac{1}{K_0^2}\, T_3(k) = \frac{m}{2\pi^2 k} \int p \frac{1}{K_0^2}\, T_2\left(p, k, -\frac{3}{4m}({q_3}^2 + k^2)\right) \ln\left(\frac{\frac{3}{4}{q_3}^2 + k^2 + p^2 - kp}{\frac{3}{4}{q_3}^2 + k^2 + p^2 + kp}\right) T_3(p) dp \qquad (8.1)$$

and then iteratively calculating the eigenvalues $\frac{1}{K_0^2}$ of the kernel. As a starting point, a well-chosen value for K_0 should be substituted in the kernel. Then the eigenvalues of the kernel are calculated and the new calculated value for $K_0$is substituted in the kernel. This procedure is then repeated until K_0 has converged to the real value. This iteration method can be used for different well-chosen starting values for K_0 which correspond to different trimer states. Furthermore, by repeating this method for more energies $-\hbar^2 q^2/m$ the Efimov spectrum can be calculated. An advantage of this iteration method is that no K_0 grid is involved, which will increase the accuracy of the method.

9. Conclusion

In the analytical part of the report s-wave scattering by a finite square well potential has been analyzed. The phase shift, scattering length, the S-matrix, the on-shell T-matrix and the half-off-shell T-matrix have been found. These calculations required the determination of the on-shell wave function. It has been shown that the scattering length of the square well potential diverges when $K_0R = \pi/2$, $3\pi/2$, $5\pi/2$, etc. and that the width of these resonances decreases when the product K_0R increases. At diverging scattering length a bound state exists with energy $E = 0$. Furthermore, analysis of the half-off-shell T-matrix has showed that this T-matrix oscillates and simultaneously decays to smaller and smaller values as you go off shell.

The off-shell two-body T-matrix for s-wave scattering by the square well potential has been found by first calculating the off-shell wave function from the off-shell analog of the Lippmann-Schwinger equation. The result is the off-shell T-matrix for s-wave scattering which depends on the momentum of the incoming wave, the momentum of the scattered wave and on the energy of the two-particle system. It is given by Eq. (6.33). This T-matrix is symmetric under the exchange of the ingoing and outgoing momenta. It is consistent with the results of H. Cheng, E. Vilallonga and H. Rabitz (Cheng et al., 1990) who calculated the fully off-shell T-matrix for scattering from the spherical hard-core plus square-well potential. Moreover, the T-matrix reduces to the on-shell and half-off-shell T-matrices for s-wave scattering by a square well potential in the right limits. Furthermore, it has been shown that it is justified to consider only the s-wave scattering contribution to the off-shell T-matrix in ultracold collisions.

An import characteristic of the off-shell T-matrix is that at higher order resonances, i.e. $K_0R = n\pi/2$ with n = 3, 5, 7, etc., the absolute maximum of the T-matrix does not occur at $k'R = 0$ even if the absolute values of kR and qR are close to zero. In this case the maximum peak occurs at $k'R = K_0R$. When the resonant condition is not fulfilled, the maximum peak still occurs $k'R = 0$ although a smaller peak at $k'R = K_0R$ is also present.

In the numerical part of the report the Efimov spectrum has been calculated for a square well potential as two-body interaction and the universality of the three-body parameter has been investigated. The numerical method has reproduced the universal scaling factor $e^{\pi/s_0} = 22.7$, but no more than two significant figures could be given. A larger K_0 grid in combination with a larger k grid would give a more accurate result for the three-body parameters although it will increase the computation time significantly. The deviation of the first scaling factor ($a_1^{(-)}/a_0^{(-)} = 18$) from the universal scaling factor 22.7 is probably the result of finite range effects, but it could also be caused by the approximations used in the STM-equation.

The three-body parameter of the lowest-energy trimer state has been found. It value is $a_0^{(-)} = -3R$, so it does not equal the universal three-body parameter $a_0^{(-)} = -9.8\,R_{vdW}$ which is experimentally observed. The fact that the universal value of the three-body parameter has not been retrieved for the resonance condition $K_0R = \pi/2$ means that the potential resonance at $K_0R = n\pi/2$ in which n is an odd number greater one, has to be studied to retrieve the universal value of $a_0^{(-)}$. After all, the three-body parameter has a universal value for deep potentials decaying faster than $1/r^6$ (Horinouchi & Ueda, 2015), so it is important that the dimensions of the square well are chosen such that this criterion is fulfilled.

A surprising result of the calculated Efimov spectrum is the absence of the parameter $a_0^{(+)}$. The energy of the lowest-energy three-body bound state does not converge to the two-body bound state energy. The effect of this phenomenon is unclear. More research should be done to understand this characteristic of the Efimov spectrum. It is very interesting whether this phenomenon is also present in

the Efimov spectrum with a square well potential as two-body interactions with higher resonance conditions ($K_0R = n\pi/2$ with n = 3, 5, 7, etc.).

Furthermore, the numerical method has been useful because it has given us insight into the influence of several parameters of the numerical method on the Efimov spectrum. If the size of the matrices is larger (i.e. increasing the number of grid points n_k), more zeroes are found at high scattering lengths. This means that more Efimov states can be identified. Moreover, it has been shown that the scaling factor of the three-body parameters $a^{(-)}$ of the two highest energy Efimov trimers often differs from the universal scaling factor 22.7. This is an artefact of the solving method. This complication is not a serious problem because we are especially interested in the lowest energy three-body bound states. After all, that is where non-universality in scaling factor will occur due to finite range effects of the interaction potential. Moreover, we are especially interested in the universality of the three-body parameter $a_0^{(-)}$ which corresponds to the lowest-lying trimer state.

Furthermore, the method has shown that the matrix size should be chosen large enough to accurately identify the first few lowest energy Efimov trimers. However, the matrix size should not be too large because the time to calculate the Efimov spectrum increases significantly.

An iterative method that can be more useful to accurately calculate the Efimov spectrum faster has been described. The advantage of this iteration method is that no K_0 grid is involved, which will increase the accuracy of the method. So the research of this bachelor thesis may first of all be continued by implementing this iteration method in Mathematica and to determine the three-body parameter $a_0^{(-)}$ with a higher accuracy.

A second continuation point involves the infinitely many values for K_0R for which the scattering length diverges. In this report the Efimov bound states have been found around the resonance condition $K_0R = \frac{\pi}{2}$. However, it has been shown that the off-shell T-matrix behaves very differently at the resonance conditions for which deeper lying two-body bound states are admitted. The effect of these deeper lying two-body bound states on the Efimov spectrum is an interesting topic for further research. These deeper lying two-body bound states could lead to the universal value of $a_0^{(-)}$ because the potential is deeper for higher values of K_0R which is a requisite to retrieve the universal value of the three-body parameter. If this is the case, the lowest energy three-body bound state shifts upward in the Efimov spectrum. As a result, it could be possible that in this case the parameter $a_0^{(+)}$ is not absent.

It has been shown in Appendix D that the simplified STM-equation (Eq. (7.1)) is not valid for deep potentials ($K_0R > \pi/2$). This means that the full STM-equation should be used to analyze the effect of deeper lying two-body bound states. Another possibility is to find another approximation which simplifies the STM-equation and which is also valid for deeper potentials.

A final continuation point focuses on finding an analytical expression of the off-shell T-matrix for a Feshbach resonance and implementing it in the STM-equation to find the Efimov trimer states. The scattering phase shift of a Feshbach resonance which includes resonant open channel interactions is given in (Kokkelmans, 2014) and can be used as a starting point.

In conclusion, this report has shown that the potential resonances of the square well potential can provide more insight into the universality of the three-body parameter. After all, it is more likely to retrieve the universal value of $a_0^{(-)}$ for deeper square well potentials. The details of the finite-range nature of the interaction play a crucial rule in the universality of the three-body parameter and this should be further investigated.

Appendix A: Justification for neglecting partial waves with nonzero angular momenta

In section 6.4 the on-shell wave function of Eq. (6.18) was reduced to Eq. (6.19) by considering only the s-wave part of Eq. (6.18). Furthermore, in Eq. (6.24) only the s-wave part of the plane wave $\langle \boldsymbol{k}'|\boldsymbol{x}'\rangle$ has been taken to calculate the T-matrix. These simplifications are justified since the phase shift δ_l for nonzero l goes much faster to zero in the low energy limit than δ_0 as was shown by Eq. (4.47). So it is justified to suppose that $\delta_l = 0$ for nonzero l. Therefore Eq. (4.45) gives $f_l(k) = 0$ for nonzero l and the on-shell wave function of Eq. (6.18) reduces to

$$\langle \boldsymbol{x}|\psi^{(+)}\rangle = \frac{\sqrt{4\pi km}}{\hbar}\frac{1}{(2\pi)^{\frac{3}{2}}}\cdot \left(e^{i\delta_0(k)}\frac{\sin(kr+\delta_0(k))}{kr} + \sum_{l>0}(2l+1)\frac{P_l(\cos\theta)}{2ik}\left(\frac{e^{ikr}}{r} - \frac{e^{-i(kr-l\pi)}}{r}\right)\right). \quad (A.1)$$

Moreover, the plane wave $\langle \boldsymbol{x}|\boldsymbol{k}\rangle$ can also be expanded in terms of Legendre polynomials. According to (Sakurai, 1994)

$$\langle \boldsymbol{x}|\boldsymbol{k}\rangle = \frac{\sqrt{4\pi km}}{\hbar}\frac{1}{(2\pi)^{\frac{3}{2}}}\sum_l (2l+1) i^l j_l(kr) P_l(\hat{\boldsymbol{k}}\cdot\hat{\boldsymbol{r}}) \quad (A.2)$$

where $j_l(kr)$ is the spherical Bessel function of order l. Now we make use of the spherical symmetry of the square well potential. For a spherical symmetric local potential V Eq. (4.24) can be written as

$$\langle \boldsymbol{x}^*|V|\boldsymbol{x}''\rangle = V(\boldsymbol{x}^*)\delta^{(3)}(\boldsymbol{x}^* - \boldsymbol{x}'') = \frac{1}{4\pi(r^*)^2}\, V(r^*)\delta(r^* - r''). \quad (A.3)$$

Therefore the T-matrix can be calculated using Eq. (4.23) and (A.3). The result is given by

$$\langle \boldsymbol{k}'|T|\boldsymbol{k}\rangle = \langle \boldsymbol{k}'|V|\psi^{(+)}\rangle = \iint \langle \boldsymbol{k}'|\boldsymbol{x}^*\rangle \frac{1}{4\pi(r^*)^2}\, V(r^*)\delta(r^* - r'')\langle \boldsymbol{x}''|\psi^{(+)}\rangle\, d^3\boldsymbol{x}^* d^3\boldsymbol{x}''. \quad (A.4)$$

Now it is possible to choose the z^*-axis parallel to $\boldsymbol{k}'$ and the z''-axis parallel to $\boldsymbol{k}$. The result is

$$\langle \boldsymbol{k}'|T|\boldsymbol{k}\rangle = \iint \langle \boldsymbol{k}'|\boldsymbol{x}^*\rangle \frac{1}{4\pi(r^*)^2}\, V(r^*)\delta(r^* - r'')\langle \boldsymbol{x}''|\psi^{(+)}\rangle (r^*)^2\, \sin\theta^*\, d\theta^* d\phi^* dr^* (r'')^2\, \sin\theta''\, d\theta'' d\phi'' dr''. \quad (A.5)$$

The θ^*- and θ''-integrals can easily be evaluated for the terms with nonzero angular momenta. According to Eq. (A.2) $\langle \boldsymbol{k}'|\boldsymbol{x}^*\rangle_l \propto P_l(\cos\theta^*)$. The only other term that could depend on θ^* is f_l. However, these are supposed to be zero for nonzero l. Since

$$\int_0^\pi P_l(\cos\theta^*)\sin\theta^*\, d\theta^* = \begin{cases} 2\ for\ l = 0 \\ 0\ for\ l > 0 \end{cases}, \quad (A.6)$$

the partial waves of $\langle \boldsymbol{k}'|\boldsymbol{x}^*\rangle$ with nonzero angular momenta do not contribute to the T-matrix. Furthermore, according to Eq. (A.1) $\langle \boldsymbol{x}''|\psi^{(+)}\rangle_l \propto P_l(\cos\theta'')$. Again, the only other term that could depend on θ'' is f_l which are supposed to be zero for nonzero l. So the partial waves of $\langle \boldsymbol{x}''|\psi^{(+)}\rangle$ with nonzero angular momenta do not contribute to the T-matrix. In conclusion, it is justified to calculate the on-shell (and half-off-shell) T-matrix of the square well potential by considering only the s-wave part of the plane wave $\langle \boldsymbol{k}'|\boldsymbol{x}^*\rangle$ and the s-wave part of the on-shell wave function.

This argument is also valid for the off-shell T-matrix because the phase shifts of the off-shell wave function can also be assumed to be zero for nonzero l. After all, the probability of penetrating the

centrifugal barrier is small for a low-energy particle in general and thus it does not notice the potential $V(r)$ inside. Furthermore, the off-shell wave function $\psi_{\boldsymbol{k}}(\boldsymbol{x}, z)$ can also be written as a sum over l in which each term can be written as a product of a r-dependent factor and a Legendre polynomial of order l ($P_l(\hat{\boldsymbol{k}} \cdot \hat{\boldsymbol{r}})$) (Cheng et al., 1990). Therefore it is justified to calculate the off-shell T-matrix of the square well potential by considering only the s-wave part of the plane wave $\langle \boldsymbol{k}' | \boldsymbol{x}^* \rangle$ and the s-wave part of the off-shell wave function.

This conclusion can be checked with the off-shell T-matrix calculated by H. Cheng, E. Vilallonga and H. Rabitz (Cheng et al., 1990). Although they calculated the off-shell T-matrix for the spherical hard-core plus square-well potential, their off-shell T-matrix can also be analyzed for the square well potential by taking the radius of the spherical hard-core to zero. This fully off-shell T-matrix calculated by H. Cheng, E. Vilallonga and H. Rabitz (Cheng et al., 1990) contains all partial-wave elements. This means that not only s-wave scattering is considered and that the off-shell T-matrix for the square well potential can be written as

$$T_{sw,off}(k', k, q) = \sum_{l=0}^{\infty} T_{l,sw,off}(k', k, q). \qquad \text{(A.7)}$$

Here $T_{l,sw,off}(k', k, q)$ are the partial-wave off-shell T-matrix elements for the square well potential. Table A.1 shows the first seven of these elements for $k' = 0.01, k = 0.011$, $q = 0.02$, $\sqrt{\frac{2mV_0}{\hbar^2}} = 1$, $R = 1$ and the angle between $\hat{\boldsymbol{k}}$ and $\hat{\boldsymbol{k}}'$ is taken to be zero. This table illustrates that for low energy scattering the main contribution to the off-shell T-matrix is given by $T_{l=0,sw,off}$.

Table A.1: First seven partial-wave off-shell T-matrix elements for the square well potential for $k' = 0.01$, $k = 0.011$, $q = 0.02$, $\sqrt{\frac{2mV_0}{\hbar^2}} = 1$, $R = 1$ *and the angle between* $\hat{\boldsymbol{k}}$ *and* $\hat{\boldsymbol{k}}'$ *is taken to be zero.*

l	$T_{l,sw,off}(k', k, q)$
0	$-(1.4 \cdot 10^{-2} + i\ 1.6 \cdot 10^{-4})$
1	$-(2.1 \cdot 10^{-7} + i\ 4.0 \cdot 10^{-14})$
2	$-(1.0 \cdot 10^{-12} + i\ 2.2 \cdot 10^{-24})$
3	$-(2.4 \cdot 10^{-18} + i\ 3.2 \cdot 10^{-35})$
4	$-(3.5 \cdot 10^{-24} + i\ 1.8 \cdot 10^{-46})$
5	$-(3.2 \cdot 10^{-30} + i\ 4.8 \cdot 10^{-58})$
6	$-(2.1 \cdot 10^{-36} + i\ 6.5 \cdot 10^{-70})$

Appendix B: Additional figures of the off-shell T-matrix

In this appendix additional figures of the momentum normalized off-shell T-matrices of the square well potential are shown.

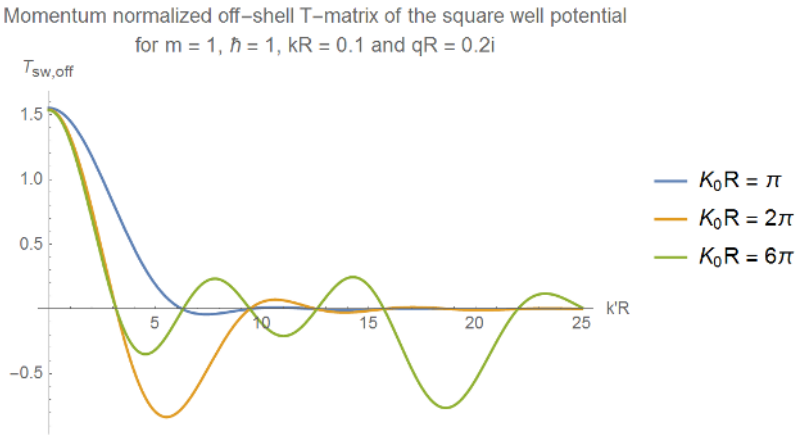

Fig. B.1. Plot of the momentum normalized $T_{sw,off}$ *versus* $k'R$ *for s-wave scattering by the square well potential with* $m = 1$, $\hbar = 1$, $qR = 0.2i$ *and* $kR = 0.1$. *The value of* K_0R *is varied. It takes the values* π, 2π *and* 6π.

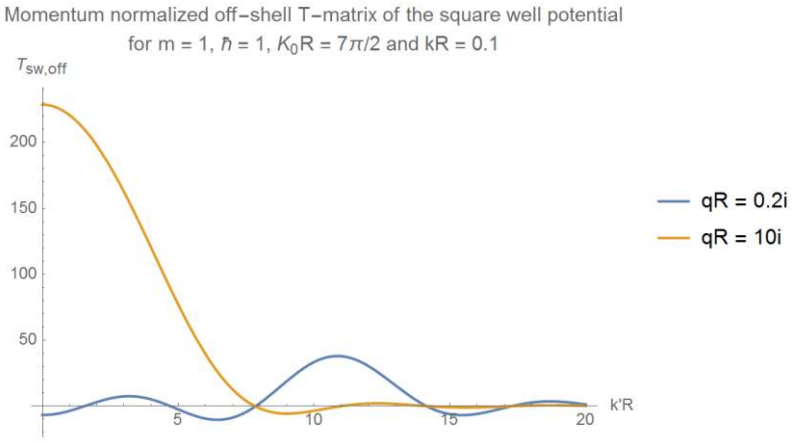

Fig. B.2. Plot of the momentum normalized $T_{sw,off}$ *versus* $k'R$ *for s-wave scattering by the square well potential with* $K_0R = 7\pi/2$ *and* $kR = 0.1$. *The value of* qR *is varied. It takes the values 0.2i, and 10i. This figure shows that for large negative energies the maximum peak occurs at* $k'R = 0$. *The peak around* $k'R = 7\pi/2 \approx 11$ *has disappeared for* $qR = 10i$.

Appendix C: Comparison with Rademaker's model

In this appendix Rademaker's off-shell T-matrix is given and compared with the off-shell T-matrix of the square well potential.

Rademaker has discussed five models with increasing complexity that describe different scattering processes (Rademaker, 2014). His second model (which is called model II in his report) describes a narrow resonance which is characterized by the scattering length a and effective range R_e. His approximated T-matrix for this scattering process is given by

$$T_{off,II}(k',k,q) = e^{-k^2/\Lambda^2} e^{-k'^2/\Lambda^2} 4\pi/m \frac{1}{\frac{1}{a} - \frac{1}{2}R_e q^2 + iq}. \tag{C.1}$$

Here the normalization condition of Eq. (5.4) has been used. Note that $T_{off,II}$ is factorized into three parts: one factor which depends only on the energy wavenumber q and two Gaussion cutoff functions of which one depends on the initial momentum k and the other depends on the final momentum k'.

In order to compare Eq. (C.1) with the off-shell T-matrix of the square well potential which is given by Eq. (6.33), we substitute the scattering length and effective range of the square well potential (i.e. Eq. (6.7) and Eq. (6.9)) in Eq. (C.1). The result is

$$T_{off,II} = e^{-(k^2+k'^2)/\Lambda^2} \frac{4\pi/m}{\frac{1}{R}\left(1-\frac{\tan KR}{KR}\right)^{-1} - Rq^2\left(1-\left(1-\frac{\tan KR}{KR}\right)^{-1} + 1/3\left(1-\frac{\tan KR}{KR}\right)^{-2}\right) + iq}. \tag{C.2}$$

In Fig. C.1, C.2 and C.3 both T-matrices are plotted. Fig. C.1 shows that both matrices decay quite similar. However, Rademaker's T-matrix does not oscillate as the wavenumber k' is varied. Fig. C.2 shows that decreasing the energy leads to a difference between both T-matrices at $k'R = 0$. This is not surprising because the expressions depend differently on the momentum wavenumber q. Furthermore, Rademaker's T-matrix is absolutely not similar to the off-shell T-matrix of the square well for $K_0R = n\pi/2$ with n = 3, 5, 7 etc. since then the maximum peak of the off-shell T-matrix is shifted which is not the case in Rademaker's model. This is shown in Fig. C.3.

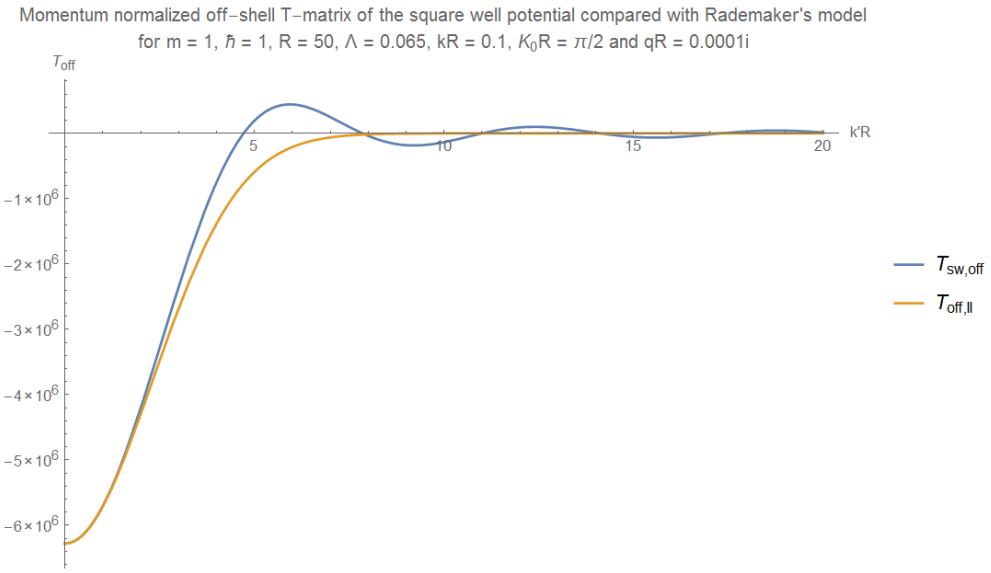

Fig. C.1. Plot of the momentum normalized T-matrices, $T_{sw,off}$ and $T_{off,II}$, versus $k'R$ for s-wave scattering by the square well potential with $qR = 0.0001i$, $K_0R = \pi/2$ and $kR = 0.1$. The cutoff parameter Λ has been chosen such that the second derivatives of both T-matrices with respect to k' are equal at $k'R = 0$.

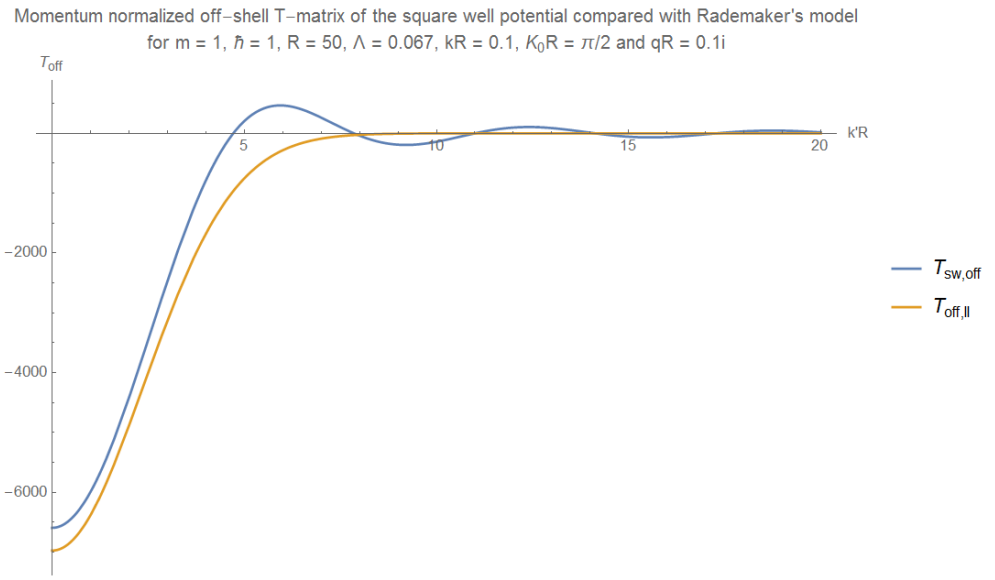

Fig. C.2. Plot of the momentum normalized T-matrices, $T_{sw,off}$ and $T_{off,II}$, versus $k'R$ for s-wave scattering by the square well potential with $qR = 0.1i$, $K_0R = \pi/2$ and $kR = 0.1$. The cutoff parameter Λ has been chosen such that the second derivatives of both T-matrices with respect to k' are equal at $k'R = 0$.

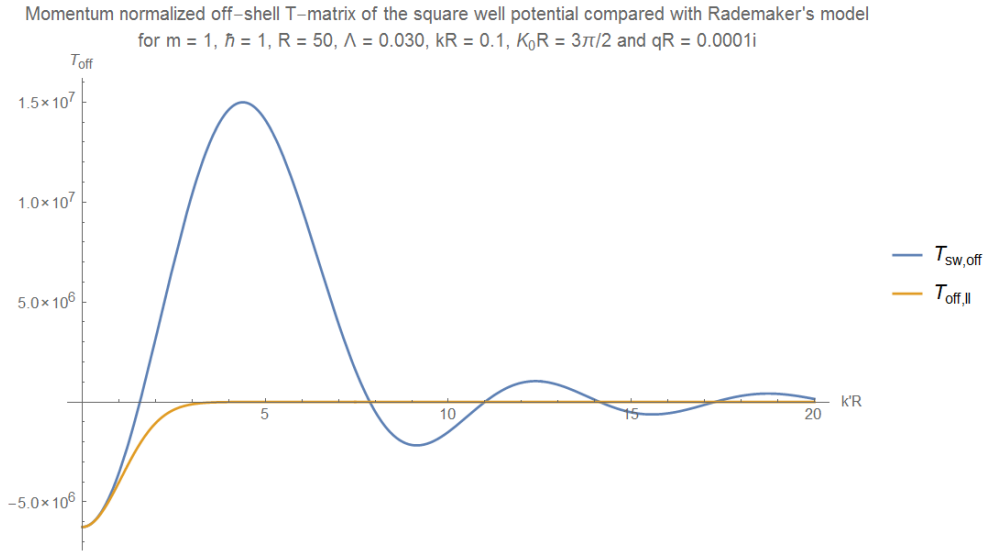

Fig. C.3. Plot of the momentum normalized T-matrices, $T_{sw,off}$ and $T_{off,II}$, versus $k'R$ for s-wave scattering by the square well potential with $qR = 0.0001i$, $K_0R = 3\pi/2$ and $kR = 0.1$. The cutoff parameter Λ has been chosen such that the second derivatives of both T-matrices with respect to k' are equal at $k'R = 0$.

Appendix D: Angular dependence of the STM-equation

D.1 Justification of Levinsen's approximation

In Eq. (7.1) the approximations $\left|\boldsymbol{k}-\frac{\boldsymbol{p}}{2}\right| \approx k$ and $\left|\boldsymbol{p}-\frac{\boldsymbol{k}}{2}\right| \approx p$ have been used. If we call θ the angle between the wavenumbers $\boldsymbol{k}$ and $\boldsymbol{p}$, we can write $\left|\boldsymbol{k}-\frac{\boldsymbol{p}}{2}\right| = \sqrt{k^2+\frac{p^2}{4}-kp\cos\theta}$ and $\left|\boldsymbol{p}-\frac{\boldsymbol{k}}{2}\right| = \sqrt{p^2+\frac{k^2}{4}-kp\cos\theta}$. Fig. D.1 shows that the momentum normalized ratio $T_{sw,off}\left(\left|\boldsymbol{p}-\frac{\boldsymbol{k}}{2}\right|,\left|\boldsymbol{k}-\frac{\boldsymbol{p}}{2}\right|,q\right)/T_{sw,off}(p,k,q)$ *with* $K_0R = \pi/2$ is only close to one for small values of pR. However, for higher values of pR the T-matrices are very different although they go both to zero. This means that high values of pR do not contribute much to the STM-equation, so in this case the approximation is not too bad.

Fig. D.2 shows that also for higher values of K_0R the ratio is only close to one for small values of pR. Both T-matrices are again very different for higher values of pR, but now the approximation fails because both T-matrices are not close to zero in the region in which they are different.

So it seems that the approximation is only valid for a square well potential with $K_0R \approx \pi/2$.

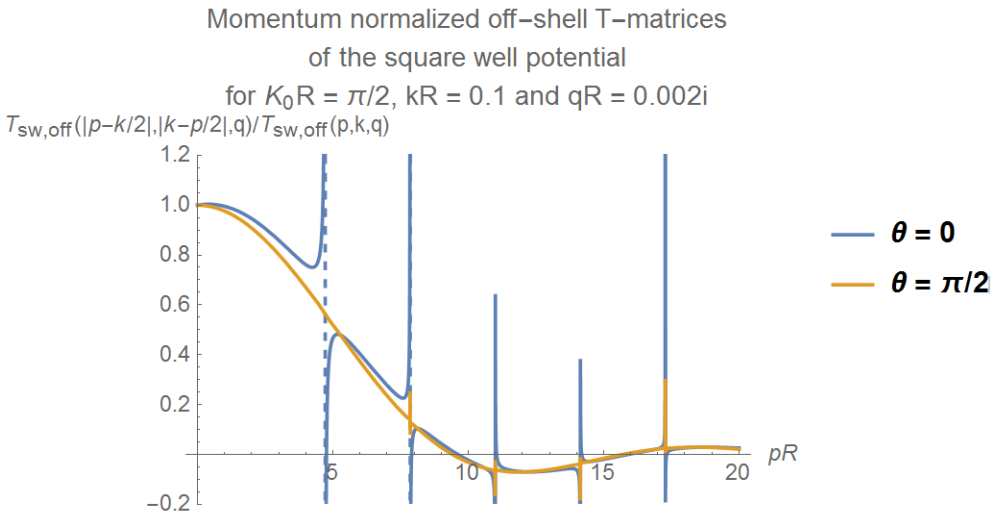

Fig. D.1. Plot of the momentum normalized ratio $T_{sw,off}\left(\left|\boldsymbol{p}-\frac{\boldsymbol{k}}{2}\right|,\left|\boldsymbol{k}-\frac{\boldsymbol{p}}{2}\right|,q\right)/T_{sw,off}(p,k,q)$ *versus* pR *for s-wave scattering by the square well potential with* $K_0R = \pi/2$. *The value of* θ *is varied. It takes the values 0 and* π.

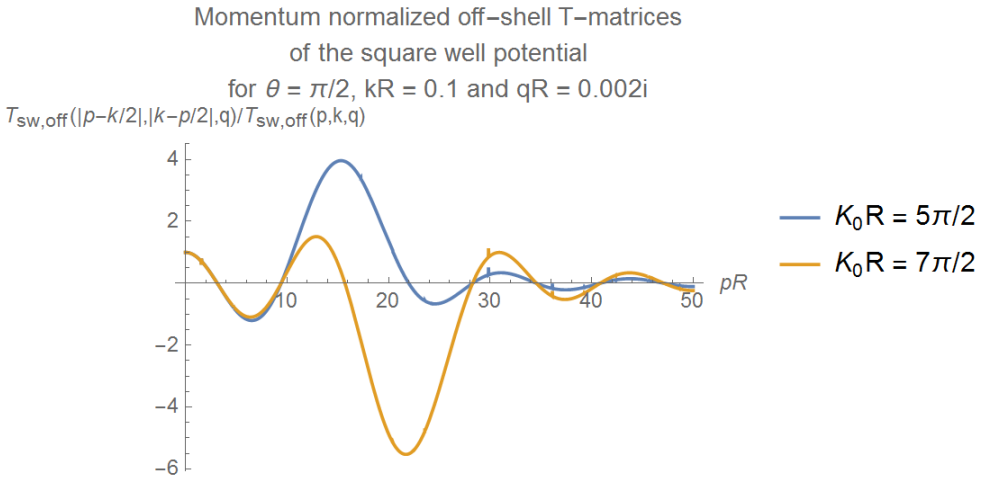

Fig. D.2. Plot of the momentum normalized ratio $T_{sw,off}(\left|\boldsymbol{p}-\frac{\boldsymbol{k}}{2}\right|,\left|\boldsymbol{k}-\frac{\boldsymbol{p}}{2}\right|,q)\,/T_{sw,off}(p,k,q)$ *versus* pR *for s-wave scattering by the square well potential with* $\theta=\pi/2$. *The value of* K_0R *is varied. It takes the values* $5\pi/2$ *and* $7\pi/2$.

D.2 Derivation of Eq. (7.1)

Starting with Eq. (5.3) and replacing $\left|\boldsymbol{k}-\frac{\boldsymbol{p}}{2}\right|$ by k and $\left|\boldsymbol{p}-\frac{\boldsymbol{k}}{2}\right|$ by p gives

$$T_3(k)=2\int\frac{d^3p}{(2\pi)^3}\frac{T_2\left(p,k,E-\frac{3k^2}{4m}\right)}{E-k^2/m-p^2/m-\boldsymbol{k}\cdot\boldsymbol{p}/m}T_3(p)$$
$$=\frac{2}{(2\pi)^3}\int_0^\infty\int_0^{2\pi}\int_0^\pi\frac{T_2\left(p,k,E-\frac{3k^2}{4m}\right)}{E-k^2/m-p^2/m-kp\cos\theta/m}T_3(p)\sin\theta\,p^2d\theta d\phi dp. \qquad \text{(D.1)}$$

Here θ is the angle between the wavenumbers $\boldsymbol{k}$ and $\boldsymbol{p}$. For s-wave scattering $T_3(k)$ and $T_2\left(p,k,E-\frac{3k^2}{4m}\right)$ do not depend on the scattering angles. Evaluating the ϕ- integral and substitution of $u=\cos\theta$ results in

$$T_3(k)=\frac{2}{(2\pi)^2}\int_0^\infty\int_{-1}^1\frac{T_2\left(p,k,E-\frac{3k^2}{4m}\right)}{E-k^2/m-p^2/m-kpu/m}T_3(p)p^2du\,dp$$
$$=-\frac{1}{2\pi^2}\frac{m}{k}\int_0^\infty T_2\left(p,k,E-\frac{3k^2}{4m}\right)\ln\left(\frac{E-k^2/m-p^2/m-kp/m}{E-k^2/m-p^2/m+kp/m}\right)p\,dp$$
$$=\frac{m}{2\pi^2k}\int_0^\infty T_2\left(p,k,E-\frac{3k^2}{4m}\right)\ln\left(\frac{E-k^2/m-p^2/m+kp/m}{E-k^2/m-p^2/m-kp/m}\right)p\,dp. \qquad \text{(D.2)}$$

This result coincides with the result of Eq. (7.1).

References

Berninger, M., Zenesini, A., Huang, B., Harm, W., Nägerl, H.-C., Ferlaino, F., Grimm, R., Julienne, P.S., Hutson, J.M. (2011). Universality of the Three-Body Parameter for Efimov States in Ultracold Cesium. *Physical Review Letters, 107*(12), 1-5.

Braaten, H., Hammer, H.-W. (2006). Universality in few-body systems with large scattering length. *Physics Reports, 428*, 259-390.

Cheng, H., Vilallonga, E., Rabitz, H. (1990). Matrix elements of the transition operator evaluated off the energy shell: Analytic results for the hard-core plus square-well spherical potential. *Physical Review A., 42*(9), 5232-5239.

Efimov, V. (1970). Energy levels arising from resonant two-body forces in a three-body system. *Physics Letters B, 33*(8), 563-564.

Ferlaino, F., Zenesini, A., Berninger, M., Huang, B., Nägerl, H.-C., Grimm, R. (2011). Efimov Resonances in Ultracold Quantum Gases. *Few-Body Systems, 51*, 113-133.

Feshbach, H. (1958). Unified Theory of Nuclear Reactions. *Annals of Physics, 5*(4), 357-390.

Griffiths, D.J. (2014). *Introduction to Quantum Mechanics.* Pearson, second edition.

Horinouchi, Y., Ueda, M. (2015). Onset of a Limit Cycle and Universal Three-Body Parameter in Efimov Physics. *Physical Review Letters, 114*(2), 1-5.

Kokkelmans, S. (2014). Feshbach resonances in ultracold gases. *World Scientific Review Volume.*

Kraemer, T., Mark, M., Waldburger, P., Danzl, J.G., Chin, C., Engeser, B., Lange, A.D., Pilch, K., Jaakkola, A., Nägerl, H.-C., Grimm, R. (2006). Evidence for Efimov quantum states in an ultracold gas of caesium atoms. *Nature, 440*, 315-318.

Landau, R.H. (1996). *Quantum Mechanics II. A Second Course in Quantum Theory.* John Wiley & Sons, Inc., second edition.

Levine, R.D. (1969). *Quantum Mechanics of Molecular Rate Processes.* Oxford University Press.

Levinsen, J. (2013). Notes on Efimov physics with different two-body interactions.

Press, W.H., Teukolsky, S.A., Vetterling, W.T., Flannery, B.P. (2007). *Numerical Recipes*. Cambridge University Press, third edition.

Rademaker, T.J. (2014). *Efimov physics for different two-body interaction models* (Bachelor thesis, Eindhoven University of Technology, the Netherlands).

Roy, S., Landini, M., Trenkwalder, A., Semeghini, G., Spagnolli, G., Simoni, A., Fattori, M., Inguscio, M., Modugno, G. (2013). Test of the Universality of the Three-Body Efimov Parameter at Narrow Feshbach Resonances. *Physical Review Letters, 111*(5), 1-5.

Sakurai, J.J. (1994). *Modern Quantum Mechanics. Revised Edition.* Addison-Wesley Publishing Company, Inc.

Schmidt, R., Rath, S.P., Zwerger, W. (2012). Efimov physics beyond universality. *The European Physical Journal B, 85*(11), 386-391.

Skorniakov, G.V., Ter-Martirosian, K.A. (1957). Three Body Problem for Short Range Forces. I. Scattering of Low Energy Neutrons by Deuterons. *Soviet Physics JETP, 4*(5), 648-661.

Taylor, J.R. (1972). *Scattering Theory: The Quantum Theory on Nonrelativistic Collisions.* John Wiley & Sons, Inc.

Thomas, L.H. (1935). The interaction between a neutron and a proton and the structure of H^3. *Physical review, 47*(12), 903.

Wild, R.J., Makotyn, P., Pino, J.M., Cornell, E.A., Jin, D.S. (2012). Measurements of Tan's Contact in an Atomic Bose-Einstein Condensate. *Physical Review Letters, 108*(14), 1-5.